

RESEARCH

Open Access



Proteomic analysis of hydrogen peroxide-treated human chondrocytes shows endoplasmic reticulum stress, cytoskeleton remodeling, and altered secretome composition

Thais Mingatos de Toledo^{1,2*}, Hellen Paula Valerio¹, Amanda Teixeira de Melo¹, Renata Nascimento Gomes¹, Thatiana Corrêa de Melo¹, Marcus Vinicius Buri¹, Marcelo Medina de Souza¹, Deivid Martins Santos², Hugo Vigerelli¹, Miryam Paola Alvarez Flores¹, Giuseppe Palmisano² and Ana Marisa Chudzinski-Tavassi^{1*}

Abstract

Background Chondrocyte homeostasis is vital for maintaining the extracellular matrix (ECM) and overall cartilage health. In osteoarthritis (OA), for example, oxidative stress resulting from redox imbalances can disrupt chondrocyte homeostasis, leading to cartilage degradation. Hydrogen peroxide (H₂O₂), a reactive oxygen species (ROS), is a key mediator of oxidative stress and contributes to chondrocyte apoptosis and ECM degradation. Previous studies have explored individual protein responses to oxidative stress; however, a comprehensive proteomic analysis in chondrocytes has not been conducted. In this study, we aimed to assess the global proteomic alterations in chondrocytes exposed to H₂O₂ using a shotgun proteomics approach, which enables the detection of a broad spectrum of proteomic changes.

Methods Chondrocytes were treated with H₂O₂ for 1, 4, and 16 h followed by protein extraction and processing, including denaturation, alkylation, and trypsin digestion. The peptides were then acidified, desalted, dried, and resuspended for LC-MS/MS. Proteomics data were analyzed using MaxQuant software to identify and quantify proteins. Secretome analysis was performed to examine protein secretion changes under oxidative stress. The statistical significance of all proteomics and secretome data was assessed using a two-tailed Student's t-test with a permutation-based FDR and an S0 parameter of 0.1 in the Perseus software. Other methods, including quantitative PCR, western blotting, and immunofluorescence, were employed to complement the proteomic analysis.

Results Our findings revealed that oxidative stress primarily affected the endoplasmic reticulum (ER), causing notable alterations in the expression of ER-associated proteins, redox-responsive enzymes, chaperones, and sialyltransferases.

*Correspondence:

Thais Mingatos de Toledo
thais.mingatos@gmail.com
Ana Marisa Chudzinski-Tavassi
ana.chudzinski@butantan.gov.br

Full list of author information is available at the end of the article



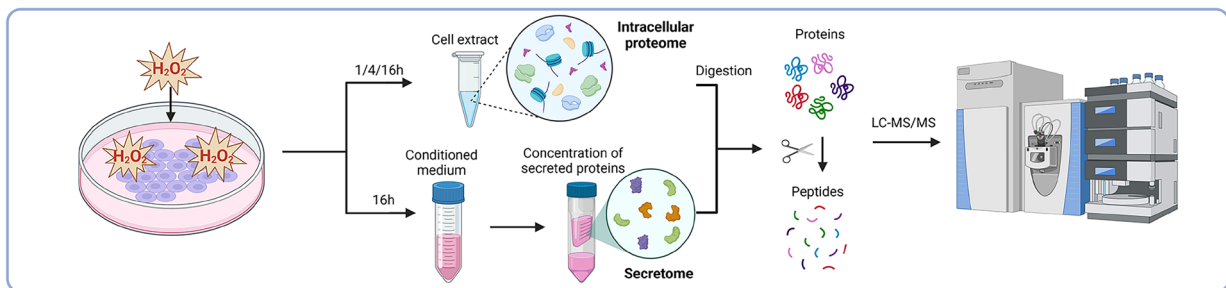
© The Author(s) 2025. **Open Access** This article is licensed under a Creative Commons Attribution-NonCommercial-NoDerivatives 4.0 International License, which permits any non-commercial use, sharing, distribution and reproduction in any medium or format, as long as you give appropriate credit to the original author(s) and the source, provide a link to the Creative Commons licence, and indicate if you modified the licensed material. You do not have permission under this licence to share adapted material derived from this article or parts of it. The images or other third party material in this article are included in the article's Creative Commons licence, unless indicated otherwise in a credit line to the material. If material is not included in the article's Creative Commons licence and your intended use is not permitted by statutory regulation or exceeds the permitted use, you will need to obtain permission directly from the copyright holder. To view a copy of this licence, visit <http://creativecommons.org/licenses/by-nc-nd/4.0/>.

These changes increased intracellular accumulation of ECM proteins and decreased secretion into the extracellular environment, indicating impaired protein trafficking and secretion. Additionally, immune-related pathways were activated in the long term, with a short-term upregulation of inflammatory markers, such as interleukin (*IL*-6 and *IL*-18), although the levels of matrix metalloproteinases (MMPs) remained stable, indicating that not only complex inflammatory stimuli, but also oxidative stress responses can disrupt ECM homeostasis.

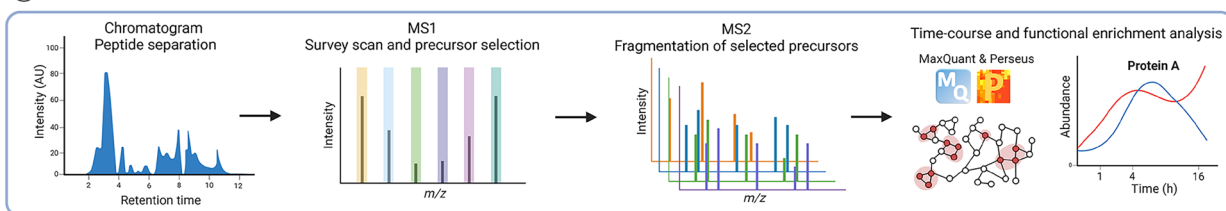
Conclusions Our study demonstrates a detailed proteomic view of the stress response of H_2O_2 -treated chondrocytes, highlighting the significant changes in ER function, cytoskeletal remodeling, protein secretion, and immune responses. These changes suggest that oxidative stress impacts ECM balance and can contribute to cartilage disorders, such as OA, through different mechanisms than what is usually observed with inflammatory stimulus, offering new insights into the molecular mechanisms underlying oxidative stress in chondrocytes.

Graphical abstract

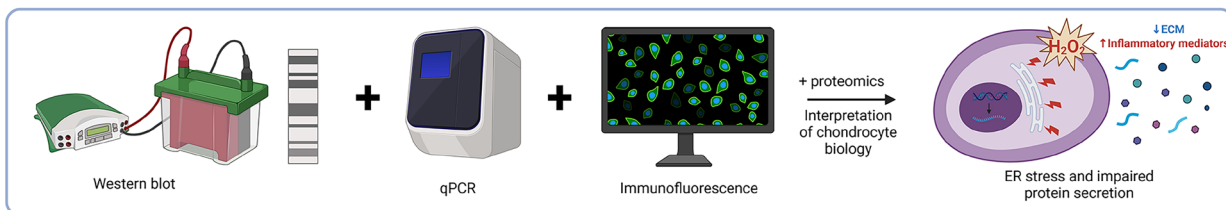
1 Overview of sample preparation for intracellular and secreted proteome analysis under oxidative stress



2 Proteomics data analysis



3 Complementary approaches to explore proteomics findings and data interpretation



Keywords Chondrocytes, Oxidative stress, Proteomics, Secretome, Osteoarthritis

Background

Chondrocyte homeostasis is crucial for maintaining the integrity of the extracellular matrix (ECM) and, consequently, cartilage health. In osteoarthritis (OA), various stress-inducing biochemical mediators trigger alterations in chondrocyte signaling and gene expression [1]. Among these, proinflammatory cytokines such as interleukin (*IL*)-1 β have been extensively studied in the context of OA. These cytokines disrupt the production of key ECM proteins, including collagen type II and aggrecan, while promoting the synthesis of matrix metalloproteinases

(MMPs), which leads to ECM degradation and further progression of OA [2]. In response to these inflammatory signals, chondrocytes adjust their physiology to the challenging microenvironment to preserve homeostasis [3, 4], which might result in oxidative stress [5].

Oxidative stress has been defined as a disturbance in the pro-oxidant/antioxidant balance, in favor of the former [6]. Reactive oxygen species (ROS) are produced in all cell types and function as cellular messengers in signal transduction, gene expression, and cell cycle regulation [7]. However, when the oxidant level exceeds the

reducing abilities of cells, ROS can lead to cellular damage through the oxidation of biomolecules, such as proteins, lipids, and DNA [8]. For instance, oxidative stress disrupts redox-sensitive organelles, including the endoplasmic reticulum (ER) [9], leading to the accumulation of misfolded proteins, which triggers ER stress and impairs protein folding, modification, and transport [10]. In addition to ER dysfunction, oxidative stress can trigger cytoskeletal remodeling and disrupt secretory pathways, which could further impair chondrocyte function [11, 12]. These disruptions contribute to the pathological remodeling of the ECM, though the exact mechanisms behind these effects remain to be elucidated [13]. Understanding how oxidative stress-induced disruptions alter the proteome of chondrocytes is essential for identifying the molecular mechanisms contributing to ECM degradation.

Due to limited oxygen availability, chondrocytes predominantly rely on glycolysis rather than mitochondrial oxidative phosphorylation for energy production [14]. Nonetheless, mitochondrial respiration continues to play a significant role by generating reactive oxygen species (ROS), which are critical for maintaining redox balance and cellular signaling in chondrocytes [15–17]. ROS can also be produced in chondrocytes through NADPH oxidase and xanthine oxidase [18, 19]. One such ROS, hydrogen peroxide (H_2O_2), is a key molecule in redox signaling and is produced in response to various stimuli, including growth factors, chemokines, and physical stress [20–22]. Cartilage exposed to H_2O_2 exhibits impaired regenerative capacity, contributing to chondrocyte apoptosis and ECM degradation [23]. Moreover, oxidative stress-induced disruptions in secretory organelles may alter the secretome of chondrocytes, impacting extracellular signaling and contributing to pathological tissue remodeling.

While previous research has predominantly focused on the role of individual proteins in response to H_2O_2 exposure [16, 24], only one proteomic study examined the global changes in chondrocytes exposed to both H_2O_2 and hyaluronic acid in 2014, identifying a limited number of protein targets [25]. Shotgun proteomics enables a comprehensive profiling of the proteome, including intracellular and secreted proteins [26, 27]. This approach is especially suited to capturing the complex remodeling of protein levels and pathways involved in chondrocyte responses to oxidative stress. Given the growing recognition of the relationship between OA, inflammatory signaling, and oxidative stress, the present study seeks to investigate the stress response of chondrocytes cultured *in vitro* under H_2O_2 exposure using a shotgun proteomics approach.

Methods

Experimental model

Commercial primary cells from human knees, Normal Human Articular Knee Chondrocytes (NHAC-Kn), were obtained from Lonza (USA) and cultured in DMEM-F12/Ham's medium (#11320033; Gibco, Netherlands) supplemented with 15 mM HEPES (#1003098482, Sigma Aldrich, USA), 10% fetal bovine serum (FBS; 12657029, Gibco, Brazil), 1 U/mL penicillin and 1 μ g/mL streptomycin (#15140122, PenStrep, Gibco, USA), at 37 °C, 5% CO_2 , and mycoplasma free.

NHAC-Kn cells were exposed to 100 μ M of H_2O_2 (#1003461059, Millipore, USA), a sub-lethal dose commonly used in the literature [28–31]. Given the short-lived nature of H_2O_2 , we examined its effects on chondrocyte protein levels through a time-series proteomics approach at 1, 4, and 16 h post-exposure, with each time point having a corresponding control.

For H_2O_2 treatment, 100 μ M H_2O_2 was added to RPMI 1640 growth medium (#1003461059, Sigma Aldrich, United Kingdom), without FBS and phenol red, supplemented with 15 mM HEPES (#1003098482, Sigma Aldrich, USA), 27.9 mM sodium bicarbonate (#101920550, Sigma Aldrich, Japan), 0.2 mM sodium pyruvate (#1002136564, Sigma Aldrich, Japan), 1 U/mL penicillin, and 1 μ g/mL streptomycin. The control group (without H_2O_2 exposure) was incubated with RPMI 1640 growth medium, without FBS and phenol red, for 1, 4, and 16 h. For each experiment, a new vial of cryopreserved cells was thawed and utilized for both control and treated cells to ensure biological consistency while minimizing batch effects. All cells were plated at passage 6 for consistency. Cell vials from a single patient were used for proteomics assays, while cell vials from at least two different patients were used for complementary techniques.

Cell lysate sample preparation

For proteomics experiments, H_2O_2 -treated cells were cultured in 150 \times 20 mm dishes until they reached 90% confluency. Afterwards, the cells were washed 3 times with PBS, scraped in 500 μ L of a lysis solution, containing 100 mM ammonium bicarbonate (Sigma Aldrich, Germany) and 1% (w/v) sodium deoxycholate (Sigma Aldrich, Italy), and lysed on ice to prevent protein degradation by intracellular proteases. Protein concentration was measured using a Pierce™ BCA Protein Assay Kit (#23227, Thermo Fisher Scientific, USA), following the manufacturer's instructions.

Secretome sample preparation

For secretome analysis, 5 mL of conditioned medium was collected from both treated and control cell cultures. The medium was concentrated using 0.5 mL Amicon® Ultra 10 kDa molecular weight cut-off filters (Millipore,

Ireland), in accordance with the manufacturer's instructions. The samples were concentrated to a final volume of 27 μL , and protein concentrations were determined using the Bradford assay (#B6916, Sigma Aldrich, USA), following the manufacturer's protocol.

Protein digestion

For cell lysates, 60 μg of protein per sample were reduced, alkylated, and digested. In the secretome experiment, 30 μg of protein per sample followed the same protocol. Reduction was performed with 5 mM dithiothreitol for 1 h at room temperature (25 °C) with agitation (800 rpm). Subsequently, proteins were alkylated with 15 mM iodoacetamide in the dark for 30 min at room temperature. Digestion was carried out overnight by adding two aliquots of trypsin (first at a 1:40 w/w ratio of trypsin and second at a 1:50 w/w ratio, with a 4-hour interval between additions) at 37 °C with agitation (800 rpm). Digestion was stopped by adding 4% trifluoroacetic acid (TFA) (#12191502, Sigma Aldrich, USA) to each sample to a final concentration of 1%. Sodium deoxycholate (#3581950, Sigma Aldrich, Italy) was precipitated by TFA addition, and the samples were centrifuged for 15 min at 14,000 $\times g$; the supernatants containing tryptic peptides were collected. Subsequently, peptides were desalted using in-house made stage-tips containing SDB-XC membranes (#66884-U, Supelco, USA), and the samples were vacuum-dried using a centrifugal concentrator (Eppendorf, USA). Briefly, the samples were washed three times with water and eluted in 70% acetonitrile (#741857, Sigma Aldrich, USA). Finally, the peptides were dissolved in 25 μL of aqueous buffer containing 0.1% formic acid (#1209246, Sigma Aldrich, Germany) for LC-MS/MS analysis.

LC-MS/MS measurements

LC-MS/MS analysis was performed for each sample using a nanoLC EASY 1200 system (LC-030378, Thermo Scientific, USA) coupled to a Q Exactive Plus mass spectrometer (03893 L, Thermo Scientific, USA) at the Mass Spectrometry Unit of CENTD (Instituto Butantan, Brazil). Peptide mixtures from each sample were injected into an Acclaim PepMap100 C18 trap column (3 μm particle size, 100 \AA pore size, 75 μm internal diameter, and 20 mm column length), which was connected to an analytical Acclaim PepMap column (2 μm particle size, 100 \AA pore size, 150 mm length, and 50 μm internal diameter), with a flow rate of 200 nL/min. A linear gradient of mobile phases was employed, where solvent A comprised 0.1% (v/v) formic acid (#1209246, Sigma Aldrich, Germany) and solvent B consisted of 80% (v/v) acetonitrile (#741857, Sigma Aldrich, USA) with 0.1% (v/v) formic acid. The gradient was applied as follows: 5–30% B over 50 min, 30–60% B over 13 min, and 60–100% B over

2 min, followed by a 5-minute isocratic step at 100% B. The mass spectrometer was operated in positive, data-dependent acquisition mode, initiating with a full MS scan across an m/z range of 300–2000 at a resolution of 75,000. MS/MS acquisition was performed via higher-energy collisional dissociation (HCD) for the ten most intense precursor ions, with quadrupole isolation set to a 1.4 m/z width. Fragmentation was conducted with a normalized collision energy of 30, and MS/MS scans were acquired at a resolution of 30,000. For the full MS scans, an automatic gain control (AGC) target value of 3×10^6 was utilized, with a maximum injection time of 200 ms. For the MS/MS scans, the AGC target was set to 2×10^5 , with a maximum injection time of 120 ms.

Protein identification and quantification

Raw data files were processed using MaxQuant software [32]. Protein identification was carried out employing the Andromeda search algorithm [33] against the *Homo sapiens* Uniprot database (downloaded in 2022; UP000005640). The mass tolerances for precursor ions and fragment ions were set at 4.5 ppm and 0.05 Da, respectively. Cysteine carbamidomethylation was specified as a fixed modification, while methionine oxidation and N-terminal acetylation were considered variable modifications. Trypsin was selected as the digestion enzyme, with a maximum allowance of two missed cleavages. A false discovery rate (FDR) threshold of 1% was applied for both peptide and protein identifications. Protein abundances were quantified using the MaxQuant label-free quantification (LFQ) algorithm [34], which normalizes chromatographic peak integrations. Default settings were applied for all other parameters.

Statistical analysis for the proteomics datasets

Before statistical analysis, the proteomics datasets were log-transformed. Contaminants, reverse database matches, proteins identified solely by modification sites, and proteins containing any missing values were excluded. For two-group comparisons, statistical significance was assessed using a two-tailed Student's t-test implemented in Perseus software [35], with a permutation-based FDR set at 5% and an S0 parameter of 0.1.

Time-course analysis was conducted using two approaches: (i) Hotelling's T statistic, combined with a multivariate empirical Bayes method, as implemented in the Timecourse R package [36], and (ii) a composite method based on three polynomial regression models, as implemented in the RolDE R package [37]. Both methods have been benchmarked for analyzing time-course proteomics datasets [37]. These methods generated ranked lists of features based on probabilities for differential expression over time. The ranks were then aggregated using the Robust Rank Aggregation method

Table 1 Antibodies used in this study

Antibody	Dilution	Secondary Antibody	Company (Reference)
BiP Antibody	1:500	Goat Anti-rabbit	Cell Signaling Technology (#31835)
LAMP-2 (H4B4)	1:1000	Goat Anti-mouse	Santa Cruz Biotechnology (#sc-18822)
Calreticulin	1:5000	Goat Anti-rabbit	Abcam (#ab2907)
Cathepsin L	1:5000	Goat Anti-rabbit	Abcam (#ab133641)
Cathepsin B	1:1000	Goat Anti-rabbit	Abcam (#ab214428)
HSP90	1:1000	Goat Anti-rabbit	Cell Signaling (#C45G5)
alpha-Tubulin	1:10000	Goat Anti-mouse	Sigma-Aldrich (#B512)
Anti-Ubiquitin (linkage-specific K48) antibody [EP8589]	1:1000	Goat Anti-rabbit	Abcam (#ab140601)
PDI Monoclonal Antibody (RL90)	1:1000	Goat Anti-mouse	Thermo (#MA3-019)
Goat Anti-Mouse IgG Antibody, HRP conjugate	1:500	-	Millipore (12–349)
Goat Anti-Rabbit IgG Antibody, HRP-conjugate	1:500	-	Millipore (12–348)

[38]. Differences in protein abundance over time were considered statistically significant if the p-value from the Robust Rank Aggregation method was less than 0.05.

Resulting plots were generated in the R statistical computing environment using standard libraries, including *ggplot2* for general plotting, *factoextra* for Principal Component Analysis, *corrplot* for correlation matrices, and *pheatmap* for Hierarchical Clustering.

Pathway enrichment analysis was performed using the web-based tool EnrichR [39] (<https://maayanlab.cloud/Enrichr/>), leveraging both Reactome and Gene Ontology annotations. As a complementary approach, we employed a statistical framework specifically designed to detect global alterations in the subcellular proteomes, as described by [40].

To investigate whether proteins contained signal peptides indicative of conventional secretion, we utilized Uniprot annotations. Additionally, the presence of secretory signal peptides was predicted using SignalP [41].

Indirect immunofluorescence, acquisition, and analysis

Cells were seeded into 96-well Microplate, PS, F-Bottom, μ Clear[®] plates (#655986; Greiner Bio-One GmbH, Baden-Württemberg, Germany), at a density of 0.8×10^4 cells/cm² and cultured in DMEM-F12 for three days. Following this, the cells were treated as described in the Experimental Model section. After 16 h, the cells were fixed

Table 2 Primers used in this study. “F” indicates the forward primer and “R” indicates the reverse primer

Gene	Symbol	Orientation sequence (5' à 3')	
ST3 beta-galactoside alpha-2,3-sialyltransferase 1	<i>ST3GAL1</i>	GCGACAGGATGGGAAAGAA	F
		CGAAGGAAGGGTGTGGTATAG	R
ST6 beta-galactoside alpha-2,6-sialyltransferase 1	<i>ST6GAL1</i>	GTCCTTAGACTGGGTGCTTATG	F
		CCGTAGCAACTTGAGGATAGAC	R
Collagen Type I Alpha 1 Chain	<i>COL1A1</i>	AGAGCATGACCGATGGATTC	F
		TGTAGGCCACGCTGTTCTTG	R
Collagen Type II Alpha 1 Chain	<i>COL2A1</i>	CTGAAACTCTGCCACCTGA	F
		TAGACGCAAGTCTGCCAGT	R
Aggrecan	<i>ACAN</i>	AAGACGGCTCCACCAGTGT	F
		ATGCCATACGCTCTCACACC	R
Interleukin 6	<i>IL6</i>	TGGCTGAAAAAGATGGATGC	F
		CACAGCTTGGCTTGTTCCT	R
Interferon Regulatory Factor 8	<i>IL8</i>	TGGACATTTCCGAGCCATAC	F
		TCCTTGATCAGCTCGTCGAT	R
Interleukin 18	<i>IL18</i>	CGGCCTCTATTGAAGATATGAC	F
		CCATACCTCTAGGCTGGCTA	R
Matrix Metallopeptidase 1	<i>MMP1</i>	TGTTTTCTGGCCACAACCTGC	F
		CTTGGGTATCCGTGTAGCA	R
Matrix Metallopeptidase 13	<i>MMP13</i>	TGGTCCGATGTAACCTCTCTG	F
		CCCAGGAGGAAAAGCATGAG	R
Glyceraldehyde-3-Phosphate Dehydrogenase	<i>GAPDH</i>	TGCACCACCAACTGCTTAGC	F
		GGCATGGACTGTGGTCATGAG	R

with 4% paraformaldehyde for 30 min at 4°C and then washed twice with 1× PBS. Permeabilization was achieved using a 0.1% Triton[™] X-100 (X100-500ML; Sigma-Aldrich, MO, USA) solution for 15 min, at 4°C, followed by two washes with 1×PBS. The cells were then blocked with 5% bovine serum albumin (BSA; A7906-50G; Sigma-Aldrich, MO, USA) for 40 min at room temperature. After blocking, cells were incubated overnight with the primary antibody β -Catenin primary monoclonal Rabbit antibody (1:250; Cell Signaling #8480, MA, USA). The next day, the cells were incubated for 1 h with Alexa Fluor[™] 488-conjugated goat anti-rabbit IgG (A21245) secondary antibody. Afterward, the cells were washed with PBS, and the nuclei were stained with Hoechst 33,342 (0.1 mg/mL; H3570, Life Technologies Corporation, NY, USA). The cells were imaged using an SP8 confocal microscope (Leica Microsystems, Hesse, Germany) scanning along the x, y, and z axes. Images were acquired using the ImageXpress[®] Micro Confocal system (Molecular Devices, San Jose, CA, USA) with an S Plan Fluor 40x/0.6 NA objective lens. DAPI was imaged using DAPI filters (Excitation 377/50 nm and Emission 447/60 nm) with a 15 ms exposure time, while β -Catenin was imaged using FITC filters (Excitation 475/34 nm and Emission 536/40 nm) with a 1000 ms exposure time. Image analysis was performed using CellProfiler[™] version 4.2.5 (www.cellprofiler.org) to segment the nuclei, β -Catenin, and cytoplasm, and quantify cell area, eccentricity, and

perimeter. Immunofluorescence was assessed across two independent experiments. Statistical comparisons were conducted using the Mann–Whitney U-test in Prism version 8 (GraphPad Software, CA, USA). Data are presented as mean \pm standard deviation and statistical significance was determined at a p-value of less than 0.05.

Western blot analysis

Western blot analysis was performed as described before [42]. Proteins extracted from cell lysates using lysis buffer were quantified using the Pierce™ BCA Protein Assay Kit (Thermo Fisher Scientific, USA), following the manufacturer's instructions. A total of 20 μ g of protein per sample was separated using SDS-PAGE and electro-transferred onto Immuno-Blot® PVDF Membrane (##1620177, Bio-Rad, CA, USA). Membranes were blocked with 5% BSA (##9048-46-8, Sigma-Aldrich, MO, USA) in Tris-buffered saline (##1610716, Bio-Rad, CA, USA) containing 0.05% Tween-20 (##9005-64-5, Sigma-Aldrich, MO, USA) (TBST) for 1 h at room temperature. Subsequently, membranes were incubated overnight at 4 °C with the respective primary antibodies diluted in a blocking solution (Table 1).

Following overnight incubation, membranes were washed three times with TBST and then incubated with secondary antibodies diluted in a blocking solution for 1 h at room temperature. Protein bands were detected using SuperSignal™ West Pico PLUS Chemiluminescent substrate kit (##77-86-1, Thermo Scientific, ON, CA) and images were obtained using the ChemiDoc XRS Imaging System. After image background adjustment, protein levels were determined by calculating the chemiluminescent bands' volume density using ImageJ software (National Institutes of Health). Statistical analysis of protein band intensities between groups was conducted using an unpaired t-test (**** $p < 0.0001$; *** $p < 0.001$; ** $p < 0.005$; * $p < 0.05$) after the normality test. Graphs were generated using GraphPad Prism version 8.1 software.

Quantitative real-time PCR (qPCR) analysis

Total RNA was extracted from cultured cells using the Illustra™ RNAspin Mini kit (GE Healthcare, Germany) following the manufacturer's protocol. cDNA was synthesized from 0.5 μ g of total SuperScript™ III First-Strand Synthesis SuperMix™ (#18080400, Invitrogen, USA) and gene-specific primers designed by the CENTD group (Table 2). The qPCR assays were performed on the QuantStudio 3 FLEX Real-Time PCR system (#A23131, Life Technologies, USA) in an 8 μ L reaction volume. Each reaction contained 4 μ L of PowerUp™ SYBR Green Master Mix (#4385612, Applied Biosystems, USA) 2 μ L of diluted cDNA (50 ng), and 2 μ L of a mix containing gene-specific forward and reverse primers (400 nM). The standard thermal cycling conditions for all transcripts

were as follows: an initial denaturation at 95 °C for 20 s, followed by 40 cycles of 95 °C for 1 s, 60 °C for 20 s, and 1 cycle of 95 °C for 1 s. A post-PCR melt curve analysis was performed to assess amplification specificity. For analysis of the expression data, the gene expression data was captured and normalized by the expression level of the housekeeping gene GAPDH. The gene expression levels of different conditions were then compared by the nonparametric Mann–Whitney U-test using GraphPad Prism version 8.1 software, p-Values less than 0.05 were considered significant. The experiment was repeated three times to ensure reproducibility.

Results

Characterization of the chondrocyte phenotype at passage 6 (P6) with mass spectrometry

To address potential concerns regarding chondrocyte dedifferentiation in monolayer culture, we performed an initial phenotypic characterization of the cells used in this study. qPCR and immunofluorescence analyses confirmed COL2 expression at P3 and P6, with fibroblasts serving as negative controls. Although COL2 levels declined and COL1 increased at P6, the continued presence of COL2 supports the retention of essential chondrocytic features. These results are shown in Figure S1 of the Supplementary File– Chondrocyte Phenotype.

To complement this characterization, we analyzed the raw mass spectrometry data using both MaxQuant and Proteome Discoverer. In both searches, we incorporated oxidized proline as a variable modification due to its established role in collagen structure. Including proline oxidation enabled confident identification of COL2A1 using both softwares. Additionally, given that phenotypic identity relies on the combined expression of multiple markers, we identified additional chondrocyte-associated proteins in our proteomics datasets. Supporting tables including full details about the markers are provided in the Supplementary File - Chondrocyte Phenotype (Tables S1–S2). Detection of chondrocytic markers was further improved in Proteome Discoverer relative to MaxQuant, likely due to its more efficient utilization of MS/MS spectra during peptide and protein identification (see the percentages of MS/MS used for peptide identification by each software in the Supplementary File - Chondrocyte Phenotype, Tables S3–S4). Overall, these results support the chondrocyte-like phenotype of the cultured cells.

An overview of temporal proteomic changes induced by H₂O₂ in human chondrocytes

We identified and quantified 2918 protein groups in all samples, using MaxQuant and considering an FDR of 1% at the peptide and protein levels (the number of proteins identified and quantified per sample are shown in Additional file 1; Figure S1A). The measurement of protein

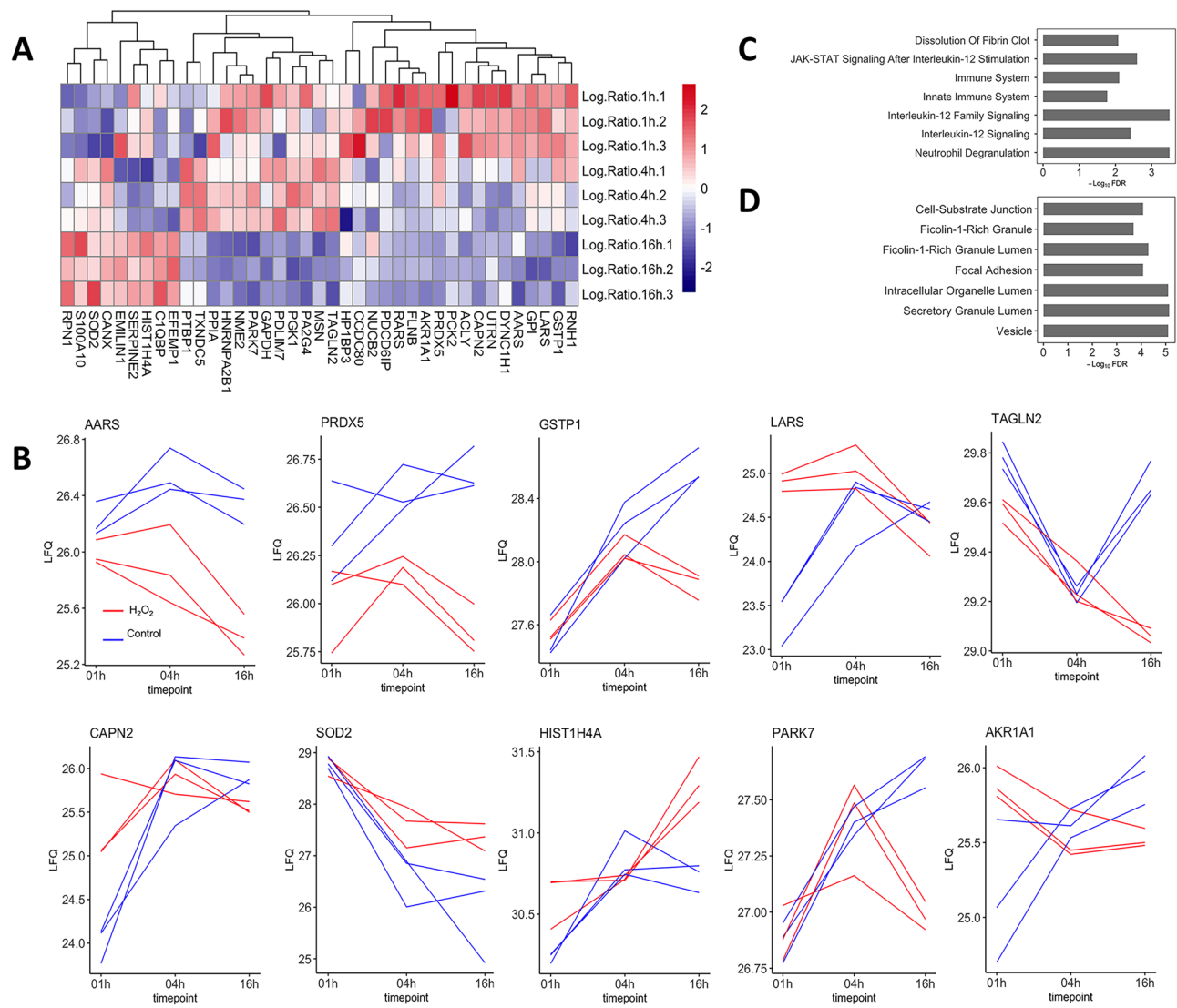


Fig. 1 Time-dependent alterations in protein abundance triggered by 100 μM of hydrogen peroxide in human chondrocytes. **A**, Hierarchical clustering of time-dependent alterations (p -value < 0.05) in NHAC-Kn cells after exposure to hydrogen peroxide ($n = 3$). The color gradient represents z-scored fold changes and columns represent replicates of the different time points. **B** and **C**, Enrichment analysis based on Reactome and Gene Ontology (GO; Cellular Component) terms, respectively, for the differentially modulated proteins displayed in the hierarchical clustering analysis. The bar plot shows the 7 most enriched Reactome pathways and GO terms and their respective FDRs. **D**, Line plots of the \log_2 LFI intensities of proteins showing time-dependent alterations in treated samples relative to controls ($n = 3$, top 10 proteins with the lowest p -values). LFI, label-free quantification

abundance exhibited high reproducibility, with correlation coefficients exceeding 0.9 within replicates of the same group (Additional file 1; Figure S1B). To ensure the quality of the quantitative dataset, all missing values inherent in data-dependent acquisition proteomics datasets were filtered out before statistical analysis. Principal component analysis demonstrated homogeneity between replicates and heterogeneity between time points (Additional file 1; Figure S1C).

Investigation of general patterns of time-dependent alterations in protein abundance using the Timecourse and RolDE R packages [36, 37] showed 39 proteins with significantly altered levels over time. Unsupervised

hierarchical clustering of these proteins revealed two main clusters of differentially regulated proteins (Fig. 1A). Detailed time-dependent alterations in abundance for the most significantly regulated proteins are presented in Fig. 1B, highlighting the change in protein dynamics over time, particularly for those associated with the response to redox imbalance (e.g., PRDX5, GSTP1, and SOD2). The complete list of significantly altered proteins, along with enriched pathways and cellular components is shown in Additional file 2; Table S1.

Next, we conducted an enrichment analysis based on Reactome terms for the significantly modulated proteins to systematically evaluate the biological implications of

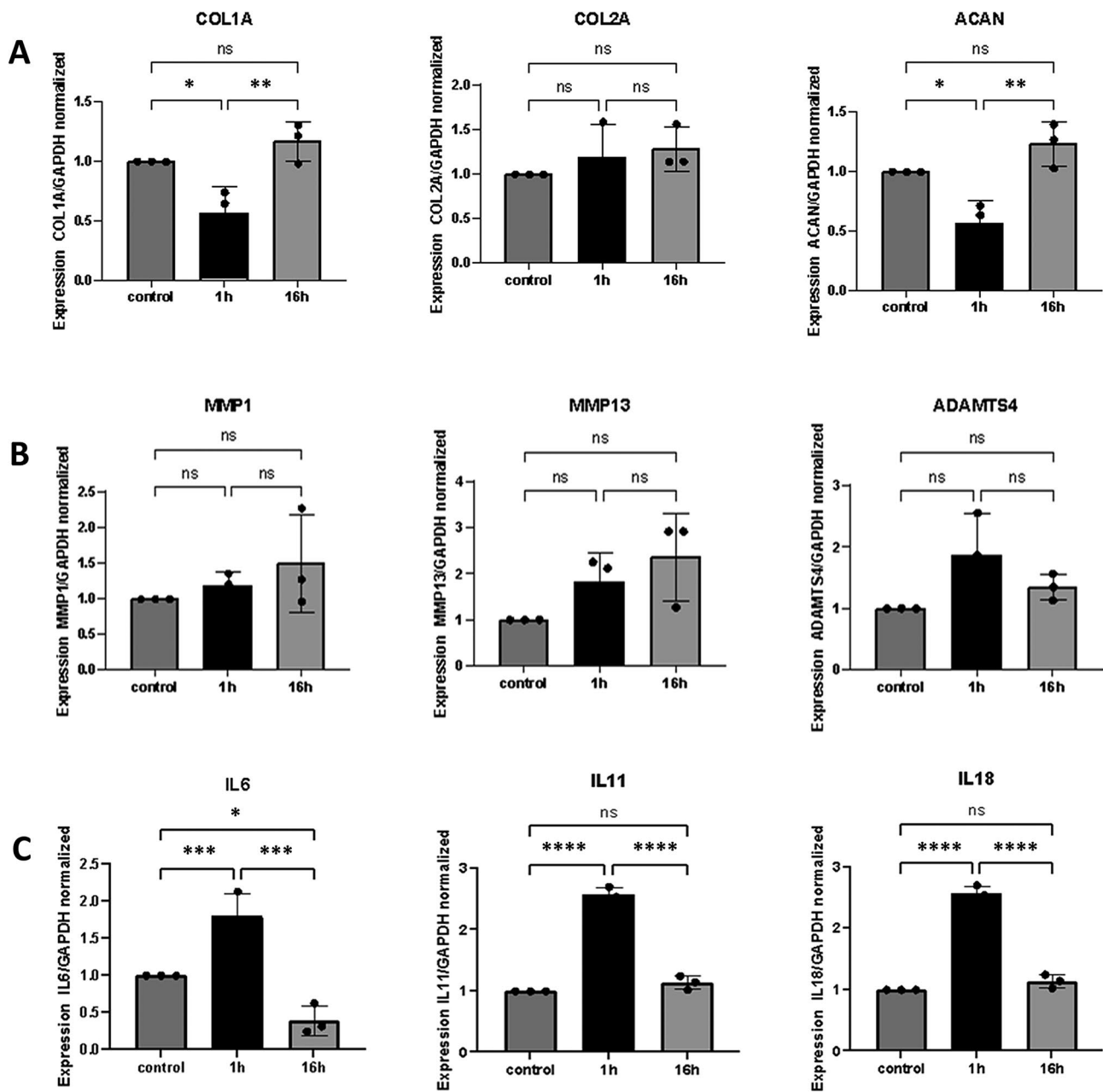


Fig. 2 Gene expression analysis in chondrocyte monolayer cells stimulated by H₂O₂ using quantitative real-time PCR (qPCR). **A**, **B**, and **C**. Bar plot shows a differential expression of ECM genes, including collagen (COL1A and COL2A), aggrecan (ACAN), matrix metalloproteinase (MMP1, MMP13, and ADAMTS4), and cytokines (IL6, IL11, and IL18). GAPDH was used as an endogenous control. Data are expressed as the mean ± SD from three independent experiments; * *p* < 0.05, compared with the control group (without stimulation by H₂O₂)

the observed changes. The analysis revealed that the most enriched pathways were associated with the immune system, encompassing terms such as “Neutrophil degranulation”, “Innate immune system”, and “Interleukin-12 Family Signaling” (the seven most enriched processes are shown in Fig. 1C as an example). Proteins associated with these processes predominantly included those involved in the redox response (e.g., GSTP1, TXNDC5, PRDX6, and SOD2), which reflects the cellular response

typically triggered by H₂O₂ treatment [43]. We also identified PPIA upregulated over shorter time-points (1 h and 4 h) and downregulated at 16 h, a protein more directly associated with inflammation, upon oxidative stress this protein is secreted via vesicular pathways mediated by cytoskeleton remodeling, contributing to proinflammatory signaling [44, 45]. Additionally, enrichment analysis based on GO terms related to subcellular localization confirmed that the significantly regulated proteins were

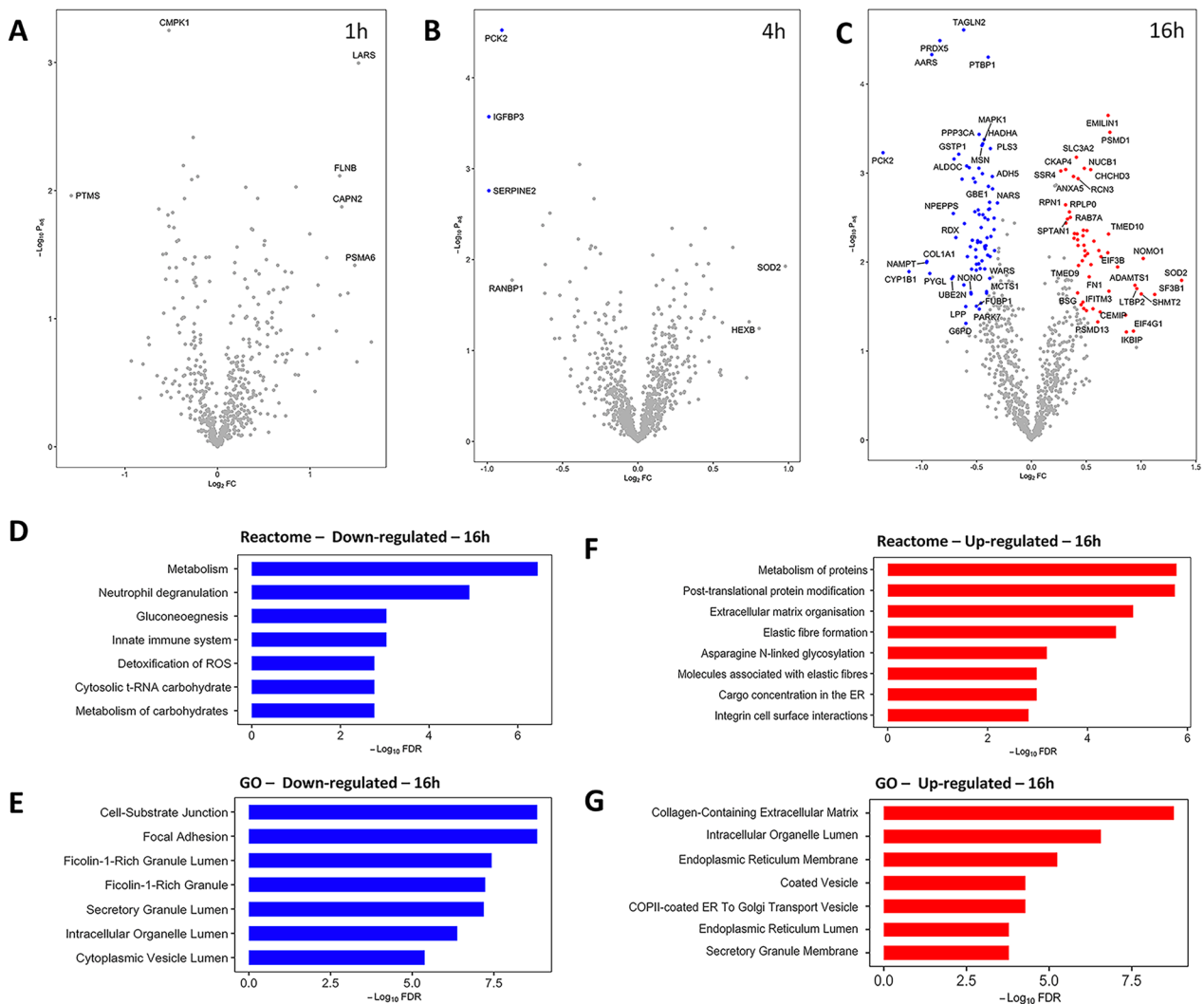


Fig. 3 Time point-specific changes in protein levels triggered by hydrogen peroxide in human chondrocytes. **A**, **B**, and **C**. Volcano plots showing differentially abundant proteins in NHAC-Kn cells after treatment with 100 μ M of hydrogen peroxide for 1, 4, and 16 h, respectively ($n_{\text{control}} = 3$, $n_{\text{H}_2\text{O}_2} = 5$). Significantly up- and downregulated proteins are highlighted in red and blue, respectively. Significance was defined by Perseus software with an FDR value of 0.05 and $S_0 = 0.1$. Labels displaying gene names are shown for proteins with the highest fold changes. **D** and **E**. Enrichment analysis based on Reactome and GO (Cellular Component) terms, respectively, for the down-regulated proteins 16 h post-exposure to hydrogen peroxide. The bar plot shows the 7 most enriched Reactome pathways and GO components, as well as their respective FDRs. **F** and **G**. Enrichment analysis based on Reactome and GO (Cellular Component) terms for the up-regulated proteins 16 h post-exposure to hydrogen peroxide. The bar plot shows the 7 most enriched Reactome pathways and GO components, as well as their respective FDRs

enriched in secreted structures and focal adhesion components (Fig. 1D).

H₂O₂ alters cellular metabolism and the production of ECM in chondrocytes

In healthy cartilages, the balance between ECM production and breakdown is tightly controlled [46]. Both collagen and aggrecan (ACAN) are key components of the ECM and hallmarks of chondrocyte phenotype. In this study, we observed a significant decrease in the expression of ACAN after 1 h of H₂O₂ stimulation, while that of collagen type II alpha (COL2A) showed no significant

alteration (Fig. 2A). Furthermore, the expression levels of MMP1, MMP13, and ADAMTS4 showed no alterations (Fig. 2B). This finding indicated that H₂O₂ can induce ACAN degradation, as previously reported [47], but does not influence the expression of MMPs, suggesting that ECM degradation by proteolytic activity might not be directly dependent on H₂O₂-induced oxidative stress. Therefore, we assessed the effects of H₂O₂ exposure on the expression of pro-inflammatory cytokines, such as IL-6, IL-11, and IL-18. The results revealed significant increases in the expression of all three cytokines after 1 h of exposure to H₂O₂ (Fig. 2C), an inflammatory effect

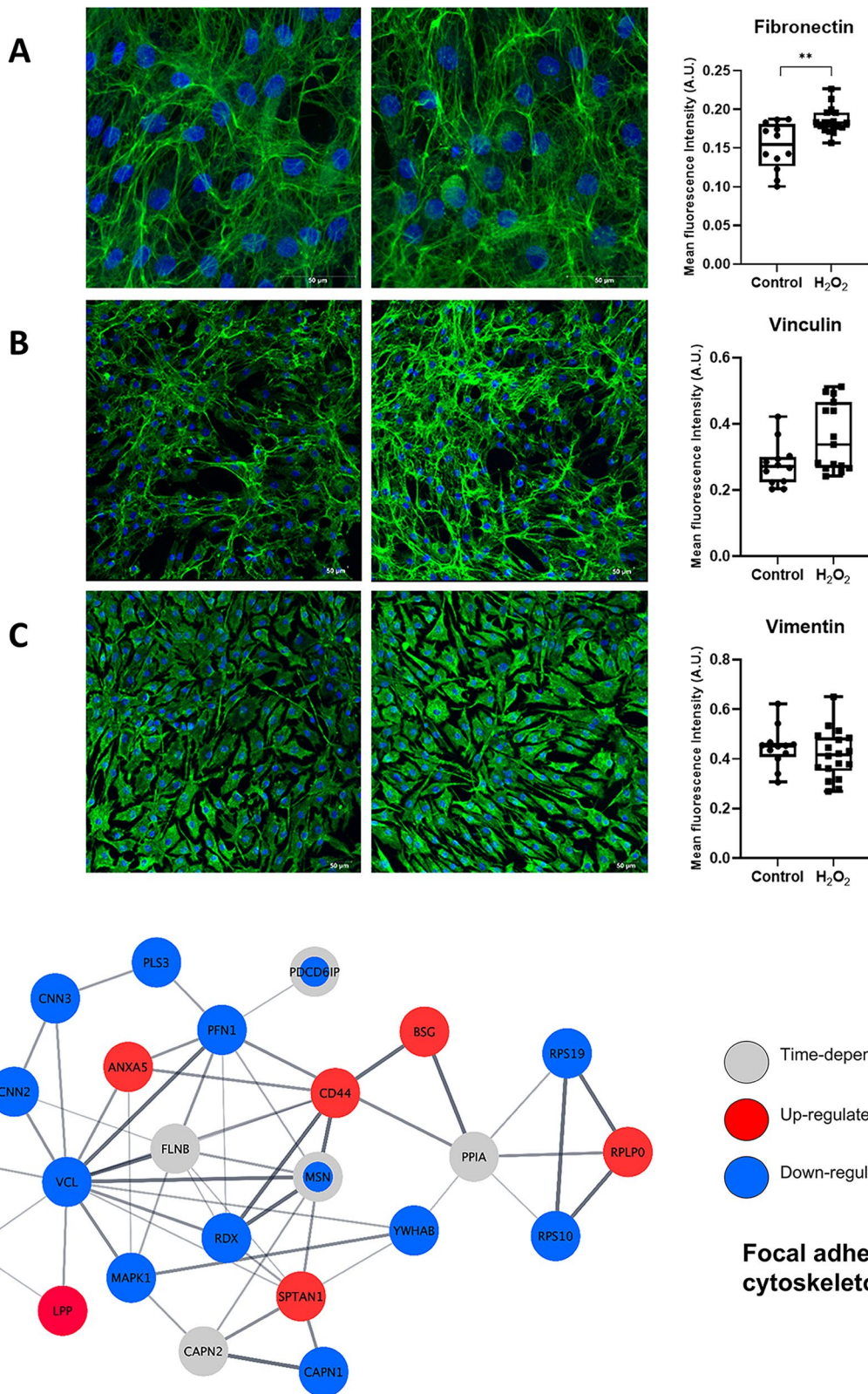


Fig. 4 (See legend on next page.)

(See figure on previous page.)

Fig. 4 Hydrogen peroxide contributes to cytoskeleton remodeling in human chondrocytes. Immunofluorescence of chondrocytes was used to visualize morphology aspects after H₂O₂ treatment. **A.** Image of chondrocytes stained with DNA probe DAPI to visualize nuclei (blue) and Alexa fluor 488 secondary antibody to visualize Fibronectin (green). Scale bar 100 μ m. **B.** Image of chondrocytes stained with DNA probe DAPI to visualize nuclei (blue) and Alexa fluor 488 secondary antibody to visualize Vinculin (green). Scale bar 100 μ m. **C.** Image of chondrocytes stained with DNA probe DAPI to visualize nuclei (blue) and Alexa fluor 488 secondary antibody to visualize Vimentin (green). Scale bar 100 μ m. **D.** String network displaying protein-protein interactions between cytoskeleton proteins with altered fold changes across time or differential abundance between biological conditions at specific time points. The selection of cytoskeleton and cell adhesion proteins was based on GO annotation

that is not typically observed at later time points following hydrogen peroxide exposure [1]. Instead, inflammatory mediators have been described to induce metabolic stress in chondrocytes [48].

To gain a more detailed understanding of the proteome remodeling induced by H₂O₂ in chondrocytes, we investigated changes in protein levels that were specific to each time point. Analysis of the protein abundances between treated samples and controls (FDR-corrected p -value < 0.05; S_0 parameter = 0.1) revealed no significant changes in cells lysed 1 h after exposure to H₂O₂ (Fig. 3A). However, at 4 h post-exposure, three proteins — PCK2, SERPINE2, and IGFBP3 — were significantly downregulated (Fig. 3B). A more extensive effect was observed at 16 h post-exposure, with 54 proteins upregulated and 79 proteins downregulated (Fig. 3C). A complete list of these significantly altered proteins, along with their enriched pathways and cellular components, is shown in Additional file 3; Table S2.

Enrichment analysis of the altered proteins revealed that the downregulated proteins were associated with Reactome terms such as “metabolism”, “innate immune system”, “neutrophil degranulation”, and “gluconeogenesis” (Fig. 3D), corroborating the previously observed roles of altered metabolism and immune response in H₂O₂-exposed chondrocytes. The proteins enriched for immune-related pathways included metabolic and redox-responsive enzymes (PRDX5, GSTP1, ALDOC, PYGB, and PYGL) as well as cytoskeletal proteins (CNN2, CNN3, VCL, and CAPN1). Additionally, LGALS3 and HMGB1, directly related to acute inflammatory responses [49, 50], were also present in this subset. GO term enrichment analysis for the downregulated proteins revealed changes in cellular junctions, focal adhesion, and secretory granules (Fig. 3E).

Conversely, the upregulated proteins were enriched for pathways related to “ECM organization” and “elastic fiber formation”, reinforcing the role of H₂O₂ in modulating ECM components (Fig. 3F). This subset of proteins included well-known ECM proteins (FBN1 and FN1), and ECM modulators (LOX and ADAMTS1). Moreover, BSG and CD44 were also identified in this subset. BSG functions as a receptor for PPIA [51], identified as responsive to H₂O₂ in the time-series analysis, while CD44 promotes chondrocyte adhesion to ECM components and actin-mediated cytoskeleton reorganization [52, 53].

Furthermore, we explored a network of significantly modulated proteins related to the cytoskeleton, cell surface signaling, and adhesion (Fig. 4). These processes were significantly enriched in both our time-series and time-point-specific analyses, including terms such as ‘Cell-substrate junction,’ and ‘Focal Adhesion.’

To investigate whether the changes in cytoskeletal proteins affecting plasma membrane interactions led to morphological alterations, we conducted immunofluorescence assays using fibronectin, vinculin, and vimentin (Fig. 4). Fibronectin levels were elevated in treated cells compared to controls, consistently with our proteomics findings. Although proteomics indicated differential regulation of vimentin, immunofluorescence intensity quantification did not show statistical significance between control and treated conditions ($p = 0.0529$) (Fig. 4). This may be due to the low statistical power of the nonparametric test used for the immunofluorescence dataset, indicating that experiments with a larger number of patients are needed to elucidate the role of this specific protein in this context.

Additionally, β -Catenin was stained to delineate the plasma membrane (Additional file 4; Figure S2). However, analysis of cell area, perimeter, and eccentricity revealed no significant differences between control and H₂O₂-treated cells, suggesting that the observed cytoskeletal changes might not manifest in broad morphological alterations.

The upregulated proteins were also enriched for terms like “cargo concentration in the ER”, “integrin cell surface interactions”, “metabolism of proteins”, and “post-translational phosphorylation of proteins”, suggesting distinctive changes in proteostasis, ER function, and cell surface signaling 16 h post-H₂O₂ exposure. Furthermore, GO enrichment analysis confirmed that the upregulated proteins were primarily associated with the ECM and the ER (Fig. 3G).

ER is the main organelle affected by H₂O₂ in chondrocytes

Given that chondrocytes, as secreting cells, are particularly susceptible to ER stress [54], we conducted a STRING network analysis to examine proteins modulated by H₂O₂ that are associated with the ER according to GO. Our analysis identified stress-responsive proteins, such as TXNDC5, CALU, CANX, ERP44, PARK7, and CAPN2 in this set (Fig. 5A). These proteins have been implicated in the response to protein unfolding/

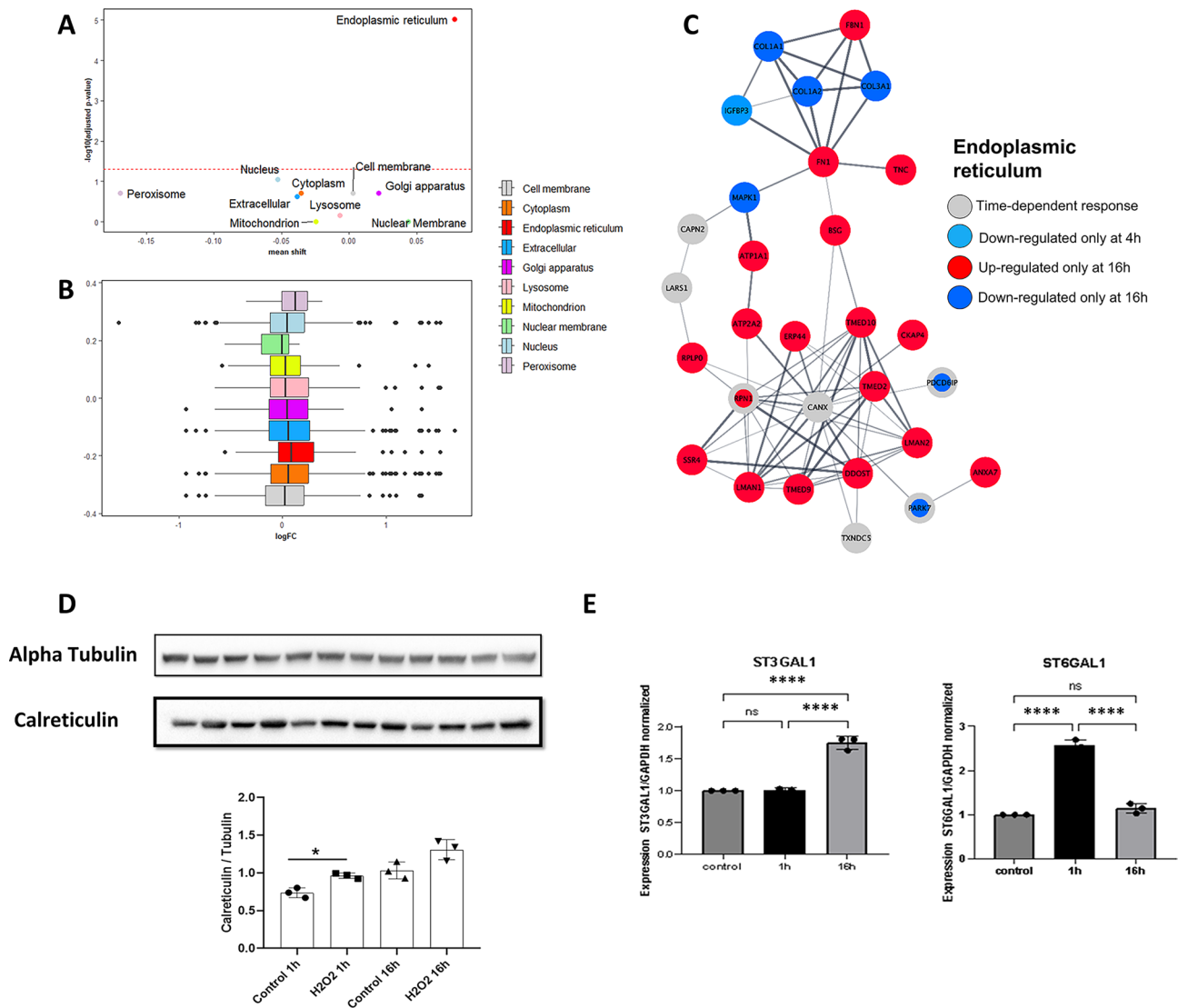


Fig. 5 Hydrogen peroxide leads to ER stress in human chondrocytes. **(A)** Compartment-specific proteomic analysis of the log₂ fold changes in hydrogen peroxide-treated NHAC-Kn cells relative to controls. Proteins were assigned to their respective compartments according to GO-terms and each compartment was tested for difference against the whole proteome (Wilcoxon rank sum test with 5% FDR correction). The y-axis displays $-\log_{10}$ Adjusted p-value and the x-axis shows the mean log₂ fold change shift. **(B)** Box plots showing the distributions of fold changes across different subcellular compartments. The fold changes were utilized for the compartment-specific proteomic analysis. **(C)** STRING network displaying protein-protein interactions between ER proteins with altered fold changes across time or differential abundance between biological conditions at specific time points. The selection of ER proteins was based on GO annotation on the STRING website. **(D)** Bar plots represent the densitometric quantification of Western blot bands for Calreticulin. Protein levels were normalized to the corresponding loading control (alpha Tubulin) and are expressed as arbitrary units in each group ($n_{\text{control}} = 3$, $n_{\text{H}_2\text{O}_2} = 3$). Data are presented as mean \pm SD from three independent experiments. Statistical significance was assessed using an unpaired student's t-test, where $p < 0.05$ was considered significant. Significant differences between control and treated groups are indicated by asterisks ($*p < 0.05$, $**p < 0.01$). **(E)** Gene expression profiles of sialyltransferases *ST3Gal1* and *ST6Gal1* were determined after 1–16 h of incubation in the presence or absence of hydrogen peroxide. Data are represented as mean \pm SD from three independent experiments and asterisks indicate significant differences between groups ($p < 0.05$)

misfolding during oxidative stress [55]. Changes in components of the ER-Golgi intermediate compartment (ERGIC) region, such as LMAN1 and LMAN2, as well as ER transport vesicles, including TMED2, TMED9, and TMED10, were also detected. Additionally, a cluster of extracellular proteins secreted through conventional and unconventional mechanisms, including FN1, FBN1, IGFBP3, and TNC, was identified. This cluster is

connected to the network through interactions with BSG and MAPK1, a signaling kinase responsive to oxidative stress [56].

Parca et al. [40]. conducted a comprehensive analysis of multiple proteomics datasets and demonstrated that proteins associated with specific subcellular compartments collectively change abundance when a given biological condition induces morphological alterations

two biological conditions. This may be due to the stringent statistical thresholds required to control for false positive rates in proteomics experiments.

For BiP, CATL, CATB, and LAMP2, we only observed subtle changes in expression levels, with a tendency toward upregulation. However, statistical significance was not achieved for these proteins, aligning with our proteomics findings for these proteins. These results suggest that while oxidative stress may induce subtle fluctuations in canonical ER and lysosomal stress markers, alternative proteins identified in our network analysis may play a more prominent role.

We also explored whether ER stress induced by H₂O₂ affects glycosylation-related gene expression in chondrocytes, considering that glycosylation is dependent on ER-Golgi function [61] and can be influenced by ER stress [62], which may modify cell surface proteins and inflammation [63]. Our results showed alterations in ST3GAL1 and ST6GAL1 expression at 16 and 1 h post-exposure, respectively. Altogether, these findings indicate that oxidative stress modulates specific ER-associated pathways in chondrocytes.

Intracellular alterations triggered by H₂O₂ in chondrocytes result in modified protein secretion

Recognizing the established role of chondrocytes as secretory cells, along with our observation of ER stress and altered production of extracellular proteins by chondrocytes over time, we conducted a chondrocyte secretome analysis to elucidate the effect of H₂O₂ on protein secretion.

In total, we identified and quantified 1458 protein groups in the conditioned medium of chondrocytes. The number of proteins identified and quantified per sample was generally higher in H₂O₂-treated samples compared to controls (Additional file 6; Figure S4A). The correlogram indicated high reproducibility, with Pearson correlation coefficients exceeding 0.9 when compared with samples from the same condition (Additional file 6; Figure S4B). In contrast, low Pearson correlation coefficients (0.2–0.4) were observed in comparison samples from different biological conditions, indicating substantial changes in secretome composition between biological conditions. The principal component analysis further confirmed this, showing a clear separation of samples from distinct conditions (Additional file 6; Figure S4C).

A total of 166 proteins were quantified across all samples, excluding missing values. Of these, 84 were annotated as “secreted” in Uniprot, while 156 were annotated as “extracellular” in GO. After 16 h H₂O₂ treatment, 117 proteins exhibited significant changes in secretion—53 were downregulated and 64 were upregulated (Student’s t-test, adjusted p-value < 0.05, S0 = 0.1; Fig. 6A).

Upregulated proteins were enriched in Reactome terms such as “neutrophil degranulation” and “immune system” (Fig. 6B). Conversely, downregulated proteins exhibited significant enrichment in terms related to ECM dynamics, including “ECM organization” and “ECM proteoglycans” (Fig. 6C).

The upregulated proteins included cytoskeletal components (VCL, ACTG1, TUBB4B, SPTAN1, FASCN1), and redox-responsive proteins and chaperones (GSTP1, HSPA1B, HSPA8, HSP90B1, TXNDC5). Proteins more directly associated with inflammation, including LGALS1, LGALS3, PPIA, and ANXA1, were also upregulated (Fig. 6D). Moreover, multiple subunits of the 14-3-3 protein were upregulated in the secretome and associated with pathways such as “SARS-CoV-2 Targets Host Intracellular Signaling and Regulatory Pathways” and “Translocation of SLC2A4 (GLUT4) to Plasma Membrane”. A specific 14-3-3 subunit (YWHAE) has been implicated as an alarmin in extracellular environments and is known to sustain OA inflammation [64].

The downregulated proteins included inhibitors of metalloproteinases (TIMP1 and TIMP2), and ECM protein modifiers (LOX, PCOLCE, QSOX1). Several structural ECM components such as fibronectin, aggrecan, decorin, lumican, osteonectin, fibromodulin, and fibulin-1 were also downregulated in response to H₂O₂ exposure (Fig. 6D). Additionally, proteins associated with the “Regulation of IGF transport”, including multiple insulin-like growth factors binding proteins (IGFBP6, IGFBP4, IGFBP3, IGFBP5, and IGFBP7) were consistently downregulated.

Even though collagen II was not consistently identified in our proteomics dataset, qPCR data showed that its expression was maintained despite monolayer culture and H₂O₂ stimulation (Supplementary File - Chondrocyte Phenotype). Meanwhile, proteomics showed the downregulation of subunits from collagens I, III, V, and XII. The complete list of significantly altered proteins, along with their enriched pathways and cellular components, is shown in Additional file 7; Table S3.

A total of 115 proteins were detected both in our intracellular and extracellular proteomics analysis. A negative correlation ($r^2 = -0.44$, p-value < 0.001) was observed between the fold changes in these datasets (Fig. 7A). Proteins exhibiting decreased intracellular abundance (fold-changes [FC] < 1) but increased secretion (FC > 1) suggest a depletion within the chondrocytes, likely due to active secretion. Conversely, proteins that accumulated intracellularly (FC > 1) but showed decreased secretion (FC < 1), indicated potential intracellular accumulation of unfolded or misfolded proteins, aligning with the observed ER stress. These findings also suggest that the potential moonlighting functions of certain proteins

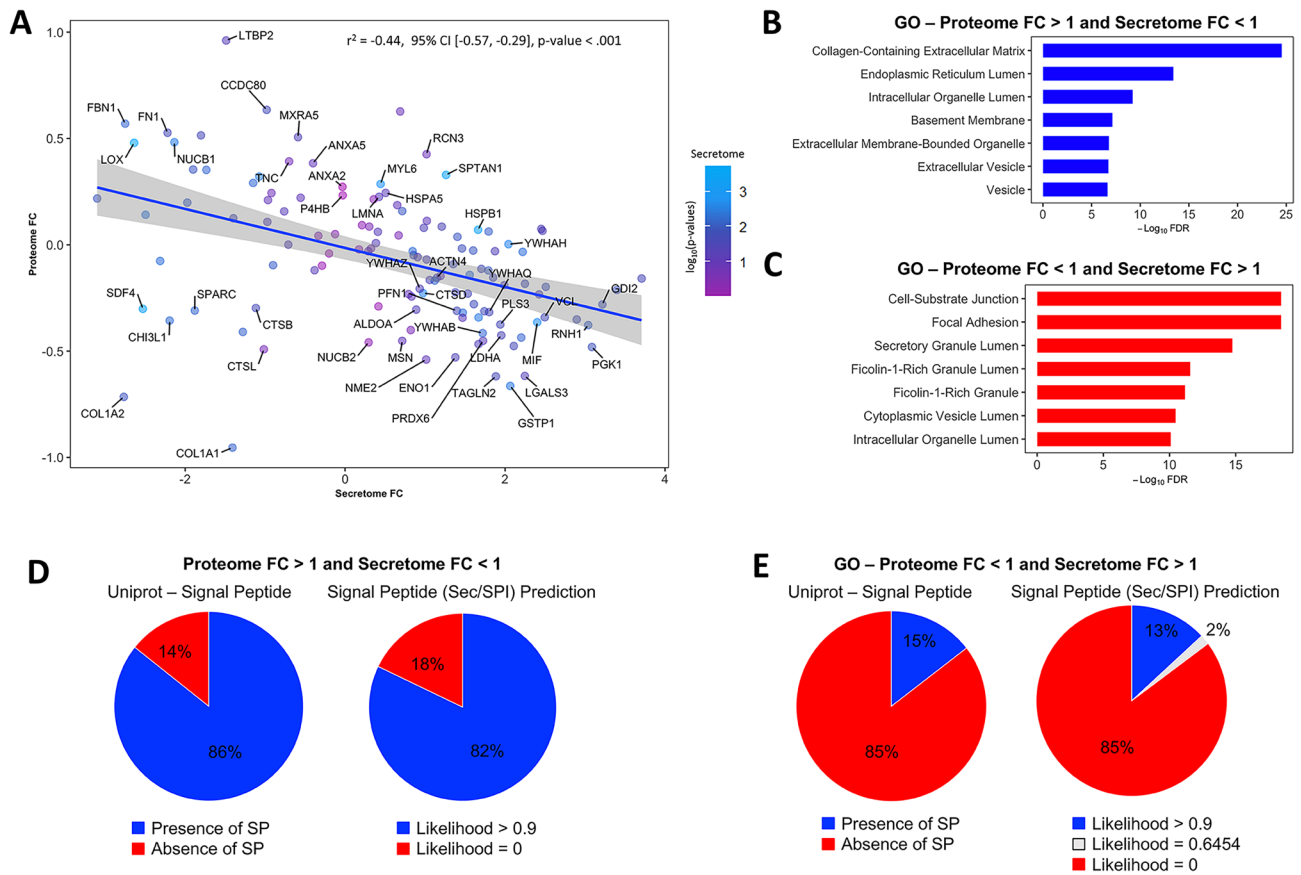


Fig. 7 Secretome analysis suggests a negative correlation between the fold changes of intracellular and extracellular proteins. **(A)** Correlation analysis between proteome and secretome fold changes for proteins detected and quantified in both datasets. The color of each data point represents the p-value of secreted protein changes compared with the control and H_2O_2 -treated samples, as indicated by the color gradient. **(B)** GO term enrichment analysis for proteins with a proteome FC > 1 and a secretome FC < 1. The bar plot shows the top seven enriched terms along with their respective FDRs. **(C)** Enrichment analysis based on GO terms for proteins found to have a proteome FC < 1 and a secretome FC > 1. The bar plot shows the 7 most enriched terms as well as their respective FDRs. **(D)** Pie charts representing the proportion of proteins with a proteome FC > 1 and a secretome FC < 1 that contain a signal peptide according to Uniprot and the likelihood of containing a signal peptide based on SignalP predictions. **(E)** Pie charts representing the proportion of proteins with a proteome FC < 1 and a secretome FC > 1 that contain a signal peptide according to Uniprot and the likelihood of containing a signal peptide based on SignalP predictions

inside and outside cells result in their differential regulation in these microenvironments [65].

To further explore these patterns, we conducted an enrichment analysis on two protein subsets: those that accumulated intracellularly (Proteome FC > 1 and Secretome FC < 1) and those efficiently secreted (Proteome FC < 1 and Secretome FC > 1). A detailed list of these proteins is provided in Additional file 8; Table S4. Proteins that accumulated intracellularly were enriched for ECM and ER (Fig. 7B), consistent with impairments in secretion due to ER stress. Specifically, 16 out of 28 proteins were classified as part of the ER in the GO database. In contrast, proteins that were efficiently secreted were significantly enriched for “Cell-substrate Junction”, “Focal Adhesion” and “Secretory Granule Lumen” (Fig. 7C).

Additionally, we examined whether proteins from these two subsets contained signal peptides indicative of conventional secretion through the ER and Golgi. Most of

the proteins that accumulated intracellularly contained a signal peptide, according to UniProt (Fig. 7D). Moreover, a high likelihood of containing a signal peptide targeting them to the extracellular environment was also identified using SignalP [41] (Fig. 7D). Conversely, both the UniProt and SignalP analyses revealed that most proteins that were efficiently secreted lacked a signal peptide (Fig. 7E), suggesting potential unconventional secretion mechanisms.

Discussion

In this study, we conducted a comprehensive proteomic analysis to elucidate the molecular responses of chondrocytes to H_2O_2 -induced oxidative stress, revealing the temporal dynamics of proteome remodeling. A previous study examining proteome changes in chondrocytes exposed to H_2O_2 identified only 13 differentially regulated proteins [25]. However, this study employed

two-dimensional gel electrophoresis (2DE), a technique with known limitations, including low sensitivity, restricted dynamic range, and gel-to-gel variability. The previous study primarily focused on the apoptotic effects of H₂O₂ and the protective role of hyaluronic acid. In contrast, our study broadens the scope by highlighting key changes in ER function, immune responses, cytoskeletal organization, and protein secretion that were further explored by western blotting, qPCR, and immunofluorescence. These findings offer a detailed characterization of cellular responses to oxidative stress, enhancing our understanding of H₂O₂-mediated damage.

The focus of this study was a time-dependent analysis of oxidative stress in human chondrocytes, combined with secretome characterization. To enable the simultaneous study of both the secretome and proteome, which required substantial amounts of cellular material, we opted for a monolayer cell culture strategy using passage 6 chondrocytes. However, this approach is known to lead to partial loss of the native phenotype of these cells, particularly when the cells are cultured in matrix-free cultures, as described by von der Mark et al. [66]. This process likely occurs because chondrocytes are sensitive and responsive to mechanical cues from their native ECM microenvironment in articular cartilage. Alternative strategies, such as matrix-mimicking systems or spheroid cell culture models using low-passage chondrocytes, which better replicate physiological conditions, could provide new insights into their response to oxidative stress, and offer advantages for studying ECM dynamics. Additionally, expanding the cohort of patients in terms of gender, age, and cell source would increase the genetic background, potentially revealing a broader range of responses. In this study, despite the limitations described, our observations highlight significant proteomic changes in chondrocytes under oxidative stress, including ER dysfunction and impaired ECM protein secretion, offering a deeper understanding of how redox imbalances affect chondrocyte function.

Despite this partial loss of native phenotype associated with extended *in vitro* culture, there is a growing interest in the use of higher-passage chondrocytes for cartilage tissue engineering [67, 68]. Therefore, we conducted a thorough characterization of the chondrocyte phenotype and demonstrated that cells at P6, although exhibiting reduced levels of COL2 compared to P3, still produce considerable levels of this protein relative to a fibroblastic negative control. Moreover, other important chondrocyte-specific proteins, such as Cartilage Oligomeric Matrix Protein, Aggrecan and Cartilage-associated Protein, are produced and secreted at significant levels by chondrocytes at P6. These findings provide further insights into the behavior of cultured chondrocytes and support our subsequent analysis.

When comparing unstimulated and hydrogen peroxide-exposed chondrocytes, our protein interaction network revealed altered levels of actin-binding proteins and those regulating interactions between actin filaments and the plasma membrane, as well as between cells and the ECM. Also, both proteomics and immunofluorescence analysis showed differential regulation for fibronectin 16 h after exposure to H₂O₂. Despite no broad alterations in cellular morphology, the changes in protein levels could still be part of the cellular response to oxidative stress [69, 70].

For instance, protein disulfide isomerase (PDI) deficiency, which induces misfolding stress in the ER, has been linked to disruptions in focal adhesions and cytoskeleton organization, particularly through the downregulation of MSN and CNN3 [70] — both of which were observed to be downregulated in our proteomic analysis. Additionally, changes in cell surface protein glycosylation, such as reduced sialylation and increased galectin-3 binding, are known to increase cytokine release in rheumatic diseases, linking cell surface alterations and inflammation [63].

Chondrocytes are subject to metabolic stresses, including oxidative stress, due to low oxygen levels and limited nutrient availability [71]. These conditions lead to the accumulation of misfolded proteins and activation of the unfolded protein response (UPR) [9], impairing protein synthesis and increasing chaperone production [72]. The buildup of mutant ECM proteins in the ER further disrupts chondrocyte function and contributes to OA progression [73]. Given that a substantial portion of proteins are secreted or transported from the ER to other organelles, maintaining ER function is crucial for proper protein secretion [74]. Impaired ER-associated degradation can lead to cartilage damage similar to OA pathology in mice, primarily due to the abnormal accumulation of ECM proteins [75].

Our proteomic analysis highlights the ER as a key target of oxidative stress in chondrocytes exposed to H₂O₂. We observed significant changes in ER-associated proteins, including redox-responsive enzymes and chaperones (e.g., TXNDC5, CALU, CANX, ERP44, and PARK7). Additionally, alterations in proteins involved in ER and ERGIC vesicles (e.g., TMED2, TMED9, TMED10, LMAN1, and LMAN2) suggest disruptions in protein trafficking and secretion. The secretome analysis corroborated these findings, showing intracellular accumulation of ER proteins, consistent with markers of ER stress.

We further explored the induction of ER stress by measuring additional ER stress markers such as calreticulin, using Western blotting. Calreticulin and PDI, in particular, have been associated with the misfolded protein accumulation in the ER and oxidative stress [60]. While we observed subtle fluctuations in canonical ER and

lysosomal stress markers, in principle H_2O_2 does not seem to lead to a robust activation of these pathways in chondrocytes. Instead, alternative proteins associated with protein trafficking, secretion and folding identified in our network analysis may play a more prominent role.

Importantly, signs of ER dysfunction identified in our proteomics dataset might contribute to broader changes in cellular function, as suggested by previous studies on glycosylation changes in chondrocytes under inflammatory stimuli, particularly involving sialic acids. Our gene expression analysis of sialyltransferases, ST3GAL1 and ST6GAL1, along with our secretome data, further corroborated these findings [76–78].

Our temporal and time-point-specific proteomic analysis revealed that chondrocytes exposed to H_2O_2 modulate the production of ECM proteins and immune mediators. In terms of ECM protein production, we observed upregulation of proteins associated with OA progression, such as LOX, which is known to drive a catabolic shift in chondrocytes and promote cartilage degeneration [79]. Similarly, we observed the intracellular upregulation of ADAMTS1 in chondrocytes 16 h post-exposure to H_2O_2 . ADAMTS1 is upregulated in OA cartilage, which promotes the degradation of ACAN [80]. Additionally, CD44, another upregulated protein, is involved in regulating chondrocyte dedifferentiation under mechanical stress [52].

The secretome analysis revealed a negative regulation of proteins essential for maintaining healthy cartilage. For example, ECM proteins crucial for cartilage structure and maintenance, such as ACAN, DCN, HSPG2, BGN, and FBLN1 were downregulated in the conditioned medium of H_2O_2 -treated cells compared to those in control cells. This finding is consistent with previous studies reporting the downregulation of ACAN and COL2A following H_2O_2 exposure [81, 82]. Further contributing to the context of ECM remodeling, TIMP1 and TIMP2, key inhibitors of MMPs, were also downregulated in the secretome of stressed cells. The downregulation of these proteins has been associated with OA progression [83]. H_2O_2 has previously been shown to reduce TIMP1 and TIMP3 expression [81].

SPARC, crucial for ECM homeostasis due to its calcium richness and interaction with collagen [84], was downregulated in the secretome of stressed cells. Reduced SPARC secretion has been linked to collagen instability and cartilage weakening [84]. Interestingly, low SPARC secretion has been observed in LRP1 knockdown models, which are associated with the progression of OA and rheumatoid arthritis [85]. Our study revealed negative regulation of LRP1-binding proteins (e.g., TIMP2, FN1, SERPINE2, MMP2, DCN, C1S, C1R, and CTSD) in chondrocytes exposed to H_2O_2 , corroborating findings from LRP1 knockdown models [85], except for PSAP,

which was downregulated in our study but upregulated in LRP1 knockdown models.

In terms of the immune response, our secretome analysis revealed enrichment of immune-related pathways under oxidative stress, with qPCR confirming increased expression of inflammatory mediators IL-6, IL-11, and IL-18 shortly after H_2O_2 treatment. While previous studies have not observed enhanced NF- κ B activation or IL-6 production in chondrocytes at later time points [1, 28], our proteomic data reveal immune pathway enrichment 16 h post-treatment, suggesting the involvement of alternative inflammatory mediators. Our temporal analysis revealed the upregulation of PPIA, a key protein associated with inflammation. PPIA is known to be secreted under oxidative stress by endothelial cells, activating pro-inflammatory signaling pathways [86]. Furthermore, PPIA was also upregulated in the secretome of H_2O_2 -exposed chondrocytes and a receptor for this protein (BSG) was upregulated at 16 h post-exposure to stress [87]. In addition, other proteins such as ANXA1, HMGB1, MIF, YWHAE, and LGALS3 emerge as potential mediators influencing the impact of oxidative stress on pro-inflammatory signaling in chondrocytes. A few of these proteins, such as HMGB1, MIF, ANXA1, and LGALS3 are secreted via unconventional pathways [88–90], which may explain why their secretion remains unaffected by ER stress.

Additionally, our data suggest a negative correlation between intracellular and extracellular protein FCs. This could reflect disruptions in the secretion of proteins that depend on the ER, as well as intracellular depletion of proteins secreted through alternative pathways. These findings emphasize the importance of studying intracellular and extracellular protein dynamics to fully understand how chondrocytes respond to oxidative stress.

Conclusions

In conclusion, our study elucidates the molecular responses of chondrocytes to H_2O_2 -induced oxidative stress, highlighting the interconnected roles of ER stress, cytoskeletal remodeling, protein secretion, and immune response that are key factors associated with the progression of OA. This comprehensive analysis identifies pathways and regulatory mechanisms that contribute to the degradation of ECM integrity and the inflammatory phenotype observed in stressed chondrocytes. Our findings reveal alterations in IL expression due to oxidative stress over a short period (1 h), while MMPs remain unchanged during this timeframe. However, ER stress and secretome analysis demonstrated disruptions in ECM protein production and secretion, suggesting that oxidative stress impairs ECM homeostasis. This disruption may contribute to poor ECM recovery and exacerbate cartilage degeneration driven by inflammatory cues

in OA. Further investigations are warranted to elucidate the specific mechanisms underlying cytoskeleton remodeling and the role of oxidative stress in driving inflammation, particularly through alterations in glycosylation and galectin-mediated pathways. These insights could pave the way for novel therapeutic strategies aimed at mitigating oxidative damage and preserving chondrocyte function in OA.

Abbreviations

ACAN	aggrecan
ACTG1	actin gamma 1
ADAMST1	a disintegrin and metalloproteinase with thrombospondin motifs 1
ADAMTS4	a disintegrin and metalloproteinase with thrombospondin motifs 4
ALDOC	aldolase C
ANXA1	annexin A1
BGN	biglycan
BiP	binding immunoglobulin protein
BSG	basigin
CALU	calumenin
CANX	calnexin
CAPN1	calpain-1
CAPN2	calpain-2
CATB	cathepsin B
CD44	cluster of differentiation 44
C1R	complement C1r subcomponent
C1S	complement C1s subcomponent
CNN2	calponin 2
CNN3	calponin 3
COL2A	collagen type II alpha
DCN	decorin
ECM	extracellular matrix
ER	endoplasmic reticulum
ERGIC	ER-Golgi intermediate compartment
FASCN1	fascin actin-bundling protein 1
FBN1	fibrillin-1
FBLN1	fibulin-1
FBS	fetal bovine serum
FC	fold change
FDR	false discovery rate
FN1	fibronectin 1
GSTP1	glutathione S-transferase pi 1
GO	gene ontology
H ₂ O ₂	hydrogen peroxide
HMGB1	high-mobility group box 1
HSP70	heat shock protein 70
HSPA1B	heat shock protein family A (Hsp70) member 1B
HSPA8	heat shock protein family A (Hsp70) member 8
HSP90B1	heat shock protein 90 beta family member 1
HSPG2	heparan sulfate proteoglycan 2
IL-1 β	interleukin-1 β
IL-6	interleukin-6
IL-8	interleukin-8
IL-18	interleukin-18
IGFBP	insulin-like growth factor binding protein
LC-MS/MS	liquid chromatography coupled to tandem mass spectrometry
LOX	lysyl oxidase
LRP1	low-density lipoprotein receptor-related protein 1
LAMP2	lysosome-associated membrane protein 2
MAPK1	mitogen-activated protein kinase 1
MIF	macrophage migration inhibitory factor
MMP	matrix metalloproteinase
MMP1	matrix metalloproteinase 1
MMP2	matrix metalloproteinase 2
MMP13	matrix metalloproteinase 13
NHAC-Kn	normal human articular knee chondrocytes
OA	osteoarthritis

PBS	phosphate-buffered saline
PCA	principal component analysis
PCK2	phosphoenolpyruvate carboxykinase 2
PCOLCE	procollagen C-endopeptidase enhancer
PDI	protein disulfide isomerase
PPIA	peptidylprolyl isomerase A
PRDX5	peroxiredoxin 5
PRDX6	peroxiredoxin 6
PYGB	glycogen phosphorylase B
PYGL	glycogen phosphorylase L
QSOX1	quiescin sulfhydryl oxidase 1
ROS	reactive oxygen species
SOD2	superoxide dismutase 2
SERPINE2	serpin family E member 2
SPARC	secreted protein acidic and rich in cysteine
SPTAN1	spectrin alpha non-erythrocytic 1
ST3GAL1	ST3 beta-galactoside alpha-2,3-sialyltransferase 1
ST6GAL1	ST6 beta-galactoside alpha-2,6-sialyltransferase 1
TFA	trifluoroacetic acid
TIMP1	tissue inhibitor of metalloproteinases 1
TIMP2	tissue inhibitor of metalloproteinases 2
TNC	tenascin
TXNDC5	thioredoxin domain-containing protein 5
UPR	unfolded protein response
VCL	vinculin
YWHAE	14-3-3 protein epsilon

Supplementary Information

The online version contains supplementary material available at <https://doi.org/10.1186/s12964-025-02291-z>.

Supplementary Material 1
 Supplementary Material 2
 Supplementary Material 3
 Supplementary Material 4
 Supplementary Material 5
 Supplementary Material 6
 Supplementary Material 7
 Supplementary Material 8
 Supplementary Material 9
 Supplementary Material 10
 Supplementary Material 11
 Supplementary Material 12

Acknowledgements

We are grateful to CAPES, FAPESP and GlaxoSmithKline for their financial support. We are also grateful to M.Sc. Rafaella M. Lafraia for technical support.

Author contributions

T.M.T conceptualized the study, T.M.T, HPV, AMC, TCM, MVB, RNG, HVB, MMS, and DMS contributed to the methodology. Formal analysis was conducted by T.M.T, HPV, AMC, TCM, and DMS. Data visualization was carried out by T.M.T, HPV, AMC, TCM, and MMS. T.M.T and HPV drafted the original manuscript. T.M.T, HPV, AMC, TCM, MPAF, GP, and AMCT contributed to the review and editing of the manuscript. GP and AMC-T supervised the project, and AMC-T secured funding.

Funding

This research was funded by FAPESP-GlaxoSmithKline (Grants 2015/50040-4, 2020/13139-0), and FAPESP-CETICs (Grant number 2013/07467-1), FAPESP, grants processes n° 2018/18257-1 (GP), 2018/15549-1 (GP), 2020/04923-0 (GP). A.M.C.-T. is a recipient of CNPq-PQ grant number 303197/2017-0 and

Fundação Butantan-PQ grants. T.M.T was a recipient of a CAPES grant. (number 88887.612671/2021-00) H.P.V is a recipient of a FAPESP grant (number 2022/01892-1). A.T.M. is a recipient of a FAPESP grant (number 2022/16532-0). Conselho Nacional de Desenvolvimento Científico e Tecnológico (“Bolsa de Produtividade” to GP).

Data availability

The proteomic datasets generated during this study have been deposited to the ProteomeXchange Consortium (<http://www.proteomexchange.org/>) via the PRIDE repository (identifier: PXD056759).

Declarations

Ethics approval and consent to participate

Not applicable.

Consent for publication

Not applicable.

Competing interests

The authors declare no competing interests.

Author details

¹Centre of Excellence in New Target Discovery, Instituto Butantan, São Paulo, Brazil

²Laboratory of Glycoproteomics, Departamento de Parasitologia, Instituto de Ciências Biomédicas, Universidade de São Paulo, São Paulo, Brazil

Received: 11 November 2024 / Accepted: 4 June 2025

Published online: 13 June 2025

References

- Yagi M, Endo K, Komori K, Sekiya I. Comparison of the effects of oxidative and inflammatory stresses on rat chondrocyte senescence. *Sci Rep*. 2023;13:7697. <https://doi.org/10.1038/s41598-023-34825-1>.
- Chow YY, Chin K-Y. The role of inflammation in the pathogenesis of osteoarthritis. *Mediators Inflamm*. 2020;2020:8293921. <https://doi.org/10.1155/2020/8293921>.
- Muttigi MS, Han I, Park H-K, Park H, Lee S-H. Matrilin-3 role in cartilage development and osteoarthritis. *Int J Mol Sci*. 2016;17:590. <https://doi.org/10.3390/ijms17040590>.
- Bello AB, Kim Y, Park S, Muttigi MS, Kim J, Park H, et al. Matrilin3/TGFβ3 gelatin microparticles promote chondrogenesis, prevent hypertrophy, and induce paracrine release in MSC spheroid for disc regeneration. *Npj Regen Med*. 2021;6:1–13. <https://doi.org/10.1038/s41536-021-00160-0>.
- Ansari MY, Ahmad N, Haqqi TM. Oxidative stress and inflammation in osteoarthritis pathogenesis: role of polyphenols. *Biomed Pharmacother*. 2020;129:110452. <https://doi.org/10.1016/j.biopha.2020.110452>.
- Sies H. Oxidative stress: concept and some practical aspects. *Antioxidants*. 2020;9:852. <https://doi.org/10.3390/antiox9090852>.
- Sinenko SA, Starkova TY, Kuzmin AA, Tomilin AN. Physiological signaling functions of reactive oxygen species in stem cells: from flies to man. *Front Cell Dev Biol* 2021;9. <https://doi.org/10.3389/fcell.2021.714370>
- Juan CA, de la Pérez JM, Plou FJ, Pérez-Lebeña E. The chemistry of reactive oxygen species (ROS) revisited: outlining their role in biological macromolecules (DNA, lipids and Proteins) and induced pathologies. *Int J Mol Sci*. 2021;22:4642. <https://doi.org/10.3390/ijms22094642>.
- Cao SS, Kaufman RJ. Endoplasmic reticulum stress and oxidative stress in cell fate decision and human disease. *Antioxid Redox Signal*. 2014;21:396–413. <https://doi.org/10.1089/ars.2014.5851>.
- Ong G, Logue SE. Unfolding the interactions between endoplasmic reticulum stress and oxidative stress. *Antioxidants*. 2023;12:981. <https://doi.org/10.3390/antiox12050981>.
- Sies H, Mailloux RJ, Jakob U. Fundamentals of redox regulation in biology. *Nat Rev Mol Cell Biol*. 2024;25:701–19. <https://doi.org/10.1038/s41580-024-0073-0-2>.
- Margittai É, Sitia R. Oxidative protein folding in the secretory pathway and redox signalling across compartments and cells. *Traffic*. 2011;12:1–8. <https://doi.org/10.1111/j.1600-0854.2010.01108.x>.
- Sanchez C, Bay-Jensen A-C, Pap T, Dvir-Ginzberg M, Quasnichka H, Barrett-Jolley R, et al. Chondrocyte secretome: a source of novel insights and exploratory biomarkers of osteoarthritis. *Osteoarthritis Cartilage*. 2017;25:1199–209. <https://doi.org/10.1016/j.joca.2017.02.797>.
- Zhang F, Zhang B, Wang Y, Jiang R, Liu J, Wei Y, et al. An extra-erythrocyte role of haemoglobin body in chondrocyte hypoxia adaption. *Nature*. 2023;622:834–41. <https://doi.org/10.1038/s41586-023-06611-6>.
- Cao Y, Zhang X, Shang W, Xu J, Wang X, Hu X, et al. Proinflammatory cytokines stimulate mitochondrial superoxide flashes in articular chondrocytes in vitro and in situ. *PLoS ONE*. 2013;8:e66444. <https://doi.org/10.1371/journal.pone.0066444>.
- Miao MZ, Su QP, Cui Y, Bahnson EM, Li G, Wang M, et al. Redox-active endosomes mediate α5β1 integrin signaling and promote chondrocyte matrix metalloproteinase production in osteoarthritis. *Sci Signal*. 2023;16:eadf8299. <https://doi.org/10.1126/scisignal.adf8299>.
- Hines MR, Gomez-Contreras PC, Liman S, Wilson AM, Lu KJ, O'Neill JA, et al. A reciprocal relationship between mitochondria and lipid peroxidation determines the chondrocyte intracellular redox environment. *Redox Biol*. 2024;75:103306. <https://doi.org/10.1016/j.redox.2024.103306>.
- Han J, Park D, Park JY, Han S. Inhibition of NADPH oxidases prevents the development of osteoarthritis. *Antioxidants*. 2022;11:2346. <https://doi.org/10.3390/antiox11122346>.
- Nasi S, Castelblanco M, Chobaz V, Ehrhchiou D, So A, Bernabei I, et al. Xanthine oxidoreductase is involved in chondrocyte mineralization and expressed in osteoarthritic damaged cartilage. *Front Cell Dev Biol*. 2021;9. <https://doi.org/10.3389/fcell.2021.612440>.
- Lepetos P, Papavassiliou AG. ROS/oxidative stress signaling in osteoarthritis. *Biochim Biophys Acta BBA - Mol Basis Dis*. 2016;1862:576–91. <https://doi.org/10.1016/j.bbadis.2016.01.003>.
- Sies H, Jones DP. Reactive oxygen species (ROS) as pleiotropic physiological signalling agents. *Nat Rev Mol Cell Biol*. 2020;21:363–83. <https://doi.org/10.1038/s41580-020-0230-3>.
- Mendes AF, Caramona MM, Carvalho AP, Lopes MC. Differential roles of hydrogen peroxide and superoxide in mediating IL-1-induced NF-κB activation and iNOS expression in bovine articular chondrocytes. *J Cell Biochem*. 2003;88:783–93. <https://doi.org/10.1002/jcb.10428>.
- Cicek E. Hydrogen peroxide induced oxidative damage on mechanical properties of the articular cartilage 2017. <https://doi.org/10.1556/1018.68.2017.4.3>
- Ansari MY, Ahmad N, Voleti S, Wase SJ, Novak K, Haqqi TM. Mitochondrial dysfunction triggers a catabolic response in chondrocytes via ROS-mediated activation of the JNK/AP1 pathway. *J Cell Sci*. 2020;133:jcs247353. <https://doi.org/10.1242/jcs.247353>.
- Yu C-J, Ko C-J, Hsieh C-H, Chien C-T, Huang L-H, Lee C-W, et al. Proteomic analysis of osteoarthritic chondrocyte reveals the hyaluronic acid-regulated proteins involved in chondroprotective effect under oxidative stress. *J Proteom*. 2014;99:40–53. <https://doi.org/10.1016/j.jprot.2014.01.016>.
- Aebersold R, Mann M. Mass-spectrometric exploration of proteome structure and function. *Nature*. 2016;537:347–55. <https://doi.org/10.1038/nature19949>.
- Knecht S, Eberl HC, Kreis N, Ugwu UJ, Starikova T, Kuster B, et al. An introduction to analytical challenges, approaches, and applications in mass Spectrometry-Based secretomics. *Mol Cell Proteom*. 2023;22. <https://doi.org/10.1016/j.mcpro.2023.100636>.
- Martin G, Andriamanalijaona R, Mathy-Hartert M, Henrotin Y, Pujol J-P. Comparative effects of IL-1β and hydrogen peroxide (H2O2) on catabolic and anabolic gene expression in juvenile bovine chondrocytes. *Osteoarthritis Cartilage*. 2005;13:915–24. <https://doi.org/10.1016/j.joca.2005.03.009>.
- Brandl A, Hartmann A, Bechmann V, Graf B, Nerlich M, Angele P. Oxidative stress induces senescence in chondrocytes. *J Orthop Res*. 2011;29:1114–20. <https://doi.org/10.1002/jor.21348>.
- Huang BK, Sikes HD. Quantifying intracellular hydrogen peroxide perturbations in terms of concentration. *Redox Biol*. 2014;2:955–62. <https://doi.org/10.1016/j.redox.2014.08.001>.
- Asada S, Fukuda K, Nishisaka F, Matsukawa M, Hamanisi C. Hydrogen peroxide induces apoptosis of chondrocytes; involvement of calcium ion and extracellular signal-regulated protein kinase. *Inflamm Res*. 2001;50:19–23. <https://doi.org/10.1007/s000110050719>.
- Cox J, Mann M. MaxQuant enables high peptide identification rates, individualized p.p.b.-range mass accuracies and proteome-wide protein quantification. *Nat Biotechnol*. 2008;26:1367–72. <https://doi.org/10.1038/nbt.1511>.
- Cox J, Neuhauser N, Michalski A, Scheltema RA, Olsen JV, Mann M. Andromeda: A peptide search engine integrated into the maxquant environment. *J Proteome Res*. 2011;10:1794–805. <https://doi.org/10.1021/pr101065j>.

34. Cox J, Hein MY, Luber CA, Paron I, Nagaraj N, Mann M. Accurate Proteome-wide Label-free quantification by delayed normalization and maximal peptide ratio extraction, termed MaxLFQ*. *Mol Cell Proteom*. 2014;13:2513–26. <https://doi.org/10.1074/mcp.M113.031591>.
35. Tyanova S, Temu T, Sinitcyn P, Carlson A, Hein MY, Geiger T, et al. The perseus computational platform for comprehensive analysis of (prote)omics data. *Nat Methods*. 2016;13:731–40. <https://doi.org/10.1038/nmeth.3901>.
36. Tai YC, Speed TP. A multivariate empirical bayes statistic for replicated microarray time course data. *Ann Stat*. 2006;34. <https://doi.org/10.1214/009053606000000759>.
37. Välikangas T, Suomi T, Chandler CE, Scott AJ, Tran BQ, Ernst RK, et al. Benchmarking tools for detecting longitudinal differential expression in proteomics data allows establishing a robust reproducibility optimization regression approach. *Nat Commun*. 2022;13:7877. <https://doi.org/10.1038/s41467-022-35564-z>.
38. Kolde R, Laur S, Adler P, Viljo J. Robust rank aggregation for gene list integration and meta-analysis. *Bioinformatics*. 2012;28:573–80. <https://doi.org/10.1093/bioinformatics/btr709>.
39. Kuleshov MV, Jones MR, Rouillard AD, Fernandez NF, Duan Q, Wang Z, et al. Enrichr: a comprehensive gene set enrichment analysis web server 2016 update. *Nucleic Acids Res*. 2016;44:W90–7. <https://doi.org/10.1093/nar/gkw377>.
40. Parca L, Beck M, Bork P, Ori A. Quantifying compartment-associated variations of protein abundance in proteomics data. *Mol Syst Biol*. 2018;14. <https://doi.org/10.15252/msb.20178131>.
41. Teufel F, Almagro Armenteros JJ, Johansen AR, Gislason MH, Piñl SI, Tsirigos KD, et al. SignalP 6.0 predicts all five types of signal peptides using protein language models. *Nat Biotechnol*. 2022;40:1023–5. <https://doi.org/10.1038/s41587-021-01156-3>.
42. Macedo-da-Silva J, Rosa-Fernandes L, Gomes V, de Santiago M, Santos VF, Molnar DM. Protein arginylation is regulated during SARS-CoV-2 infection. *Viruses*. 2023;15:290. <https://doi.org/10.3390/v15020290>.
43. Veal EA, Day AM, Morgan BA. Hydrogen peroxide sensing and signaling. *Mol Cell*. 2007;26:1–14. <https://doi.org/10.1016/j.molcel.2007.03.016>.
44. Jin Z-G, Lungu AO, Xie L, Wang M, Wong C, Berk BC. Cyclophilin A is a proinflammatory cytokine that activates endothelial cells. *Arterioscler Thromb Vasc Biol*. 2004;24:1186–91. <https://doi.org/10.1161/01.ATV.0000130664.51010.28>.
45. Suzuki J, Jin Z-G, Meoli DF, Matoba T, Berk BC. Cyclophilin A is secreted by a vesicular pathway in vascular smooth muscle cells. *Circ Res*. 2006;98:811–7. <https://doi.org/10.1161/01.RES.0000216405.85080.a6>.
46. Hui W, Young DA, Rowan AD, Xu X, Cawston TE, Proctor CJ. Oxidative changes and signalling pathways are pivotal in initiating age-related changes in articular cartilage. *Ann Rheum Dis*. 2016;75:449–58. <https://doi.org/10.1136/annrheumdis-2014-206295>.
47. Tiku ML, Gupta S, Deshmukh DR. Aggrecan degradation in chondrocytes is mediated by reactive oxygen species and protected by antioxidants. *Free Radic Res*. 1999;30:395–405. <https://doi.org/10.1080/10715769900300431>.
48. Defois A, Bon N, Charpentier A, Georget M, Gaigeard N, Blanchard F, et al. Osteoarthritic chondrocytes undergo a glycolysis-related metabolic switch upon exposure to IL-1b or TNF. *Cell Commun Signal*. 2023;21:137. <https://doi.org/10.1186/s12964-023-01150-z>.
49. Simovic Markovic B, Nikolic A, Gazdic M, Bojic S, Vucicevic L, Kosic M, et al. Galectin-3 plays an important Pro-inflammatory role in the induction phase of acute colitis by promoting activation of NLRP3 inflammasome and production of IL-1β in macrophages. *J Crohns Colitis*. 2016;10:593–606. <https://doi.org/10.1093/ecco-jcc/jjw013>.
50. Magna M, Pisetsky DS. The role of HMGB1 in the pathogenesis of inflammatory and autoimmune diseases. *Mol Med*. 2014;20:138–46. <https://doi.org/10.2119/molmed.2013.00164>.
51. Yurchenko V, Zybarch G, O'Connor M, Dai WW, Franchin G, Hao T, et al. Active site residues of cyclophilin A are crucial for its signaling activity via CD147*. *J Biol Chem*. 2002;277:22959–65. <https://doi.org/10.1074/jbc.M201593200>.
52. Sobue Y, Takahashi N, Ohashi Y, Suzuki M, Nishiume T, Kobayakawa T, et al. Inhibition of CD44 intracellular domain production suppresses bovine articular chondrocyte de-differentiation induced by excessive mechanical stress loading. *Sci Rep*. 2019;9:14901. <https://doi.org/10.1038/s41598-019-50166-4>.
53. Kawana H, Karaki H, Higashi M, Miyazaki M, Hilberg F, Kitagawa M, et al. CD44 suppresses TLR-Mediated Inflammation¹. *J Immunol*. 2008;180:4235–45. <https://doi.org/10.4049/jimmunol.180.6.4235>.
54. Briggs MD, Dennis EP, Dietmar HF, Pirog KA. New developments in chondrocyte ER stress and related diseases 2020. <https://doi.org/10.12688/f1000research.22275.1>.
55. Randriamboavonjy V, Kyselova A, Fleming I. Redox regulation of calpains: consequences on vascular function. *Antioxid Redox Signal*. 2019;30:1011–26. <https://doi.org/10.1089/ars.2018.7607>.
56. Rezatabar S, Karimian A, Rameshknia V, Parsian H, Majidinia M, Kopi TA, et al. RAS/MAPK signaling functions in oxidative stress, DNA damage response and cancer progression. *J Cell Physiol*. 2019;234:14951–65. <https://doi.org/10.1002/jcp.28334>.
57. Lakpa KL, Khan N, Afghah Z, Chen X, Geiger JD. Lysosomal stress response (LSR): physiological importance and pathological relevance. *J Neuroimmune Pharmacol*. 2021;16:219–37. <https://doi.org/10.1007/s11481-021-09990-7>.
58. Shang F, Taylor A. Ubiquitin–proteasome pathway and cellular responses to oxidative stress. *Free Radic Biol Med*. 2011;51:5–16. <https://doi.org/10.1016/j.freeradbiomed.2011.03.031>.
59. Qu J, Zou T, Lin Z. The roles of the Ubiquitin–Proteasome system in the endoplasmic reticulum stress pathway. *Int J Mol Sci*. 2021;22:1526. <https://doi.org/10.3390/ijms22041526>.
60. Antoniotti V, Bellone S, Gonçalves Correia FP, Peri C, Tini S, Ricotti R, et al. Calreticulin and PDIA3, two markers of endoplasmic reticulum stress, are associated with metabolic alterations and insulin resistance in pediatric obesity: A pilot study. *Front Endocrinol*. 2022;13. <https://doi.org/10.3389/fendo.2022.1003919>.
61. Zhang N, Zabolina OA. Critical determinants in ER-Golgi trafficking of enzymes involved in glycosylation. *Plants*. 2022;11:428. <https://doi.org/10.3390/plants11030428>.
62. Yung HW, Zhao X, Glover L, Burren C, Pang P-C, Jones CJ, et al. Perturbation of placental protein glycosylation by endoplasmic reticulum stress promotes maladaptation of maternal hepatic glucose metabolism. *iScience*. 2023;26:105911. <https://doi.org/10.1016/j.isci.2022.105911>.
63. Kissel T, Toes REM, Huizinga TWJ, Wuhler M. Glycobiology of rheumatic diseases. *Nat Rev Rheumatol*. 2023;19:28–43. <https://doi.org/10.1038/s41584-022-00867-4>.
64. Millerand M, Sudre L, Nefla M, Pène F, Rousseau C, Pons A, et al. Activation of innate immunity by 14-3-3 ε, a new potential alarmin in osteoarthritis. *Osteoarthritis Cartilage*. 2020;28:646–57. <https://doi.org/10.1016/j.joca.2020.03.002>.
65. Jeffery CJ. Protein moonlighting: what is it, and why is it important? *Philos Trans R Soc B Biol Sci*. 2017;373:20160523. <https://doi.org/10.1098/rstb.2016.0523>.
66. n Der Mark K, Gauss V, Von Der Mark H, Müller P. Relationship between cell shape and type of collagen synthesised as chondrocytes lose their cartilage phenotype in culture. *Nature*. 1977;267:531–2. <https://doi.org/10.1038/267531a0>.
67. Huang BJ, Hu JC, Athanasiou KA. Effects of passage number and post-expansion aggregate culture on tissue engineered, self-assembled neocartilage. *Acta Biomater*. 2016;43:150–9. <https://doi.org/10.1016/j.actbio.2016.07.044>.
68. Santoro R, Olivares AL, Brans G, Wirz D, Longinotti C, Lacroix D, et al. Bioreactor based engineering of large-scale human cartilage grafts for joint resurfacing. *Biomaterials*. 2010;31:8946–52. <https://doi.org/10.1016/j.biomaterials.2010.08.009>.
69. Wilson C, González-Billault C. Regulation of cytoskeletal dynamics by redox signaling and oxidative stress: implications for neuronal development and trafficking. *Front Cell Neurosci*. 2015;9. <https://doi.org/10.3389/fncel.2015.00381>.
70. Bilches Medinas D, Malik S, Yıldız-Bölükbaşı E, Borgonovo J, Saaranen MJ, Urta H, et al. Mutation in protein disulfide isomerase A3 causes neurodevelopmental defects by disturbing endoplasmic reticulum proteostasis. *EMBO J*. 2022;41:e105531. <https://doi.org/10.15252/embj.2020105531>.
71. Zheng P, Chen Q, Tian X, Qian N, Chai P, Liu B, et al. DNA damage triggers tubular endoplasmic reticulum extension to promote apoptosis by facilitating ER-mitochondria signaling. *Cell Res*. 2018;28:833–54. <https://doi.org/10.1038/s41422-018-0065-z>.
72. Rellmann Y, Dreier R. Different forms of ER stress in chondrocytes result in short stature disorders and degenerative cartilage diseases: new insights by cartilage-specific ERp57 knockout mice. *Oxid Med Cell Longev*. 2018;2018:8421394. <https://doi.org/10.1155/2018/8421394>.
73. Gualeni B, Rajpar MH, Kellogg A, Bell PA, Arvan P, Boot-Handford RP, et al. A novel transgenic mouse model of growth plate dysplasia reveals that decreased chondrocyte proliferation due to chronic ER stress is a key factor in reduced bone growth. *Dis Model Mech*. 2013;6:1414–25. <https://doi.org/10.1242/dmm.013342>.
74. Sim HJ, Cho C, Kim HE, Hong JY, Song EK, Kwon KY, et al. Augmented ERAD (ER-associated degradation) activity in chondrocytes is necessary for cartilage

- development and maintenance. *Sci Adv.* 2022;8:eabl4222. <https://doi.org/10.1126/sciadv.abl4222>.
75. Kopp MC, Larburu N, Durairaj V, Adams CJ, Ali MMU. UPR proteins IRE1 and PERK switch bip from chaperone to ER stress sensor. *Nat Struct Mol Biol.* 2019;26:1053–62. <https://doi.org/10.1038/s41594-019-0324-9>.
 76. Fuehrer J, Pichler KM, Fischer A, Giurea A, Weinmann D, Altmann F, et al. N-Glycan profiling of chondrocytes and fibroblast-like synoviocytes: towards functional glycomics in osteoarthritis. *Proteom– Clin Appl.* 2021;15:2000057. <https://doi.org/10.1002/prca.202000057>.
 77. Pabst M, Wu SQ, Grass J, Kolb A, Chiari C, Viernstein H, et al. IL-1 β and TNF- α alter the glycophenotype of primary human chondrocytes in vitro. *Carbohydr Res.* 2010;345:1389–93. <https://doi.org/10.1016/j.carres.2010.02.017>.
 78. Toegel S, Weinmann D, André S, Walzer SM, Bilban M, Schmidt S, et al. Galectin-1 couples glycobiology to inflammation in osteoarthritis through the activation of an NF- κ B-Regulated gene network. *J Immunol.* 2016;196:1910–21. <https://doi.org/10.4049/jimmunol.1501165>.
 79. Kim J-H, Lee G, Won Y, Lee M, Kwak J-S, Chun C-H, et al. Matrix cross-linking-mediated mechanotransduction promotes posttraumatic osteoarthritis. *Proc Natl Acad Sci.* 2015;112:9424–9. <https://doi.org/10.1073/pnas.1505700112>.
 80. Yang C-Y, Chanalaris A, Troeberg L. ADAMTS and ADAM metalloproteinases in osteoarthritis– looking beyond the 'usual suspects'. *Osteoarthritis Cartilage.* 2017;25:1000–9. <https://doi.org/10.1016/j.joca.2017.02.791>.
 81. Kim E-N, Lee H-S, Jeong G-S, Cudratricusxanthone O Inhibits. H2O2-Induced cell damage by activating Nrf2/HO-1 pathway in human chondrocytes. *Antioxidants.* 2020;9:788. <https://doi.org/10.3390/antiox9090788>.
 82. Zhou Z, Zhang L, Liu Y, Huang C, Xia W, Zhou H, et al. Luteolin protects chondrocytes from H2O2-Induced oxidative injury and attenuates osteoarthritis progression by activating AMPK-Nrf2 signaling. *Oxid Med Cell Longev.* 2022;2022:5635797. <https://doi.org/10.1155/2022/5635797>.
 83. Salminen HJ, Säämänen A-MK, Vankemmelbeke MN, Auho PK, Perälä MP, Vuorio EI. Differential expression patterns of matrix metalloproteinases and their inhibitors during development of osteoarthritis in a transgenic mouse model. *Ann Rheum Dis.* 2002;61:591–7. <https://doi.org/10.1136/ard.61.7.591>.
 84. Rosset EM, Bradshaw AD. SPARC/osteonectin in mineralized tissue. *Matrix Biol.* 2016;52–54:78–87. <https://doi.org/10.1016/j.matbio.2016.02.001>.
 85. Yamamoto K, Scavenius C, Meschis MM, Gremida AME, Mogensen EH, Thøgersen IB, et al. A top-down approach to uncover the hidden ligandome of low-density lipoprotein receptor-related protein 1 in cartilage. *Matrix Biol.* 2022;112:190–218. <https://doi.org/10.1016/j.matbio.2022.08.007>.
 86. Alvariño R, Alfonso A, Pérez-Fuentes N, González-Jartín JM, Gegunde S, Vieytes MR, et al. Extracellular cyclophilins A and C induce dysfunction of pancreatic microendothelial cells. *Front Physiol.* 2022;13. <https://doi.org/10.3389/fphys.2022.980232>.
 87. Bahmed K, Henry C, Holliday M, Redzic J, Ciobanu M, Zhang F, et al. Extracellular cyclophilin-A stimulates ERK1/2 phosphorylation in a cell-dependent manner but broadly stimulates nuclear factor kappa B. *Cancer Cell Int.* 2012;12:19. <https://doi.org/10.1186/1475-2867-12-19>.
 88. Popa SJ, Stewart SE, Moreau K. Unconventional secretion of annexins and galectins. *Semin Cell Dev Biol.* 2018;83:42–50. <https://doi.org/10.1016/j.semcdb.2018.02.022>.
 89. Wang Z, Zhou H, Zheng H, Zhou X, Shen G, Teng X, et al. Autophagy-based unconventional secretion of HMGB1 by keratinocytes plays a pivotal role in psoriatic skin inflammation. *Autophagy.* 2021;17:529–52. <https://doi.org/10.1080/15548627.2020.1725381>.
 90. Dankers W, Hasnat MA, Swann V, Alharbi A, Lee JP, Cristofaro MA, et al. Necrotic cell death increases the release of macrophage migration inhibitory factor by monocytes/macrophages. *Immunol Cell Biol.* 2020;98:782–90. <https://doi.org/10.1111/imcb.12376>.

Publisher's note

Springer Nature remains neutral with regard to jurisdictional claims in published maps and institutional affiliations.